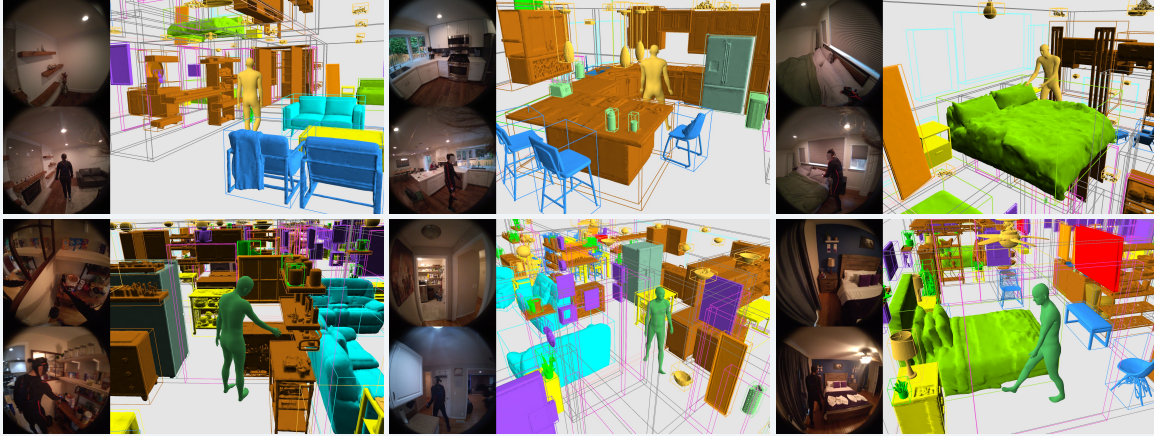


# NymeriaPlus: Enriching Nymeria Dataset with Additional Annotations and Data

Daniel DeTone\*, Federica Bogo\*, Eric-Tuan Le\*, Duncan Frost, Julian Straub, Yawar Siddiqui, Yuting Ye, Jakob Engel, Richard Newcombe, Lingni Ma

Meta Reality Labs Research

\*Equal Contribution



The Nymeria dataset [93], released in 2024, is a large-scale collection of in-the-wild human activities captured with multiple egocentric wearable devices that are spatially localized and temporally synchronized. It provides body-motion ground truth recorded with a motion-capture suit, device trajectories, semi-dense 3D point clouds, and in-context narrations. In this paper, we upgrade Nymeria and introduce NymeriaPlus. NymeriaPlus features: (1) improved human motion in Momentum Human Rig (MHR) [50] and SMPL [87] formats; (2) dense 3D and 2D bounding box annotations for indoor objects and structural elements; (3) instance-level 3D object reconstructions; and (4) additional modalities *e.g.*, basemap recordings, audio, and wristband videos. By consolidating these complementary modalities and annotations into a single, coherent benchmark, NymeriaPlus strengthens Nymeria into a more powerful in-the-wild egocentric dataset. We expect NymeriaPlus to bridge a key gap in existing egocentric resources and to support a broader range of research, including unique explorations of multimodal learning for embodied AI.

**Date:** March 20, 2026

**Correspondence:** Lingni Ma ([lingni.ma@meta.com](mailto:lingni.ma@meta.com))

**Code:** [https://github.com/facebookresearch/nymeria\\_dataset](https://github.com/facebookresearch/nymeria_dataset)

**Data:** <https://explorer.projectaria.com/nymeria>



## 1 Introduction

Recent advances in artificial intelligence (AI) have increased demand for human-centric, context-aware algorithms and systems, particularly those enabled by egocentric wearables such as smart glasses and body-worn sensors. These platforms capture multimodal signals that can provide rich context for foundation models, enabling seamless human-like understanding and interaction. An important component of this paradigm is robust, context-aware human motion understanding. Progress in this area importantly depends on large-scale datasets that combine diverse, high-quality motion with rich annotations beyond body pose, collected in natural, in-the-wild settings and spanning long-horizon activities.

The availability of egocentric datasets has grown rapidly in recent years. However, most existing benchmarks lack either reliable ground-truth human motion or sufficiently rich context annotations [82, 39, 40, 47, 103, 55, 115, 60, 104, 97, 134, 16, 133, 138, 140, 77, 66, 85, 92]. At the same time, constructing human motion datasets involves persistent trade-offs among scale, diversity, sensing modalities, and annotation quality. Although large-scale third-person motion datasets [84, 147, 49] have made notable progress by pseudo-annotating Internet videos, these pipelines do not transfer well to egocentric viewpoints. High-quality motion datasets collected in controlled environments (e.g., multi-view RGB(D) rigs or optical MoCap) provide detailed annotations but limit scene realism and the breadth of activities [145, 72, 73, 56, 22, 98]. Many motion datasets are also captured without egocentric wearables [94, 24, 139, 74, 91, 98]. Moreover, despite the strong coupling between human motion and 3D environments, most motion datasets either omit object-level annotations or lack the geometric detail needed to model human–scene interaction. A few exceptions incorporate scene context [11, 13, 104, 25, 67, 74, 108], but the environments are often synthetic or restricted to a small number of carefully mapped scenes. Conversely, many datasets provide detailed scene and object annotations [38, 142, 122, 10, 115, 149, 16, 75, 44, 41, 45] but focus on static environments without human interaction. Existing human–object interaction datasets are frequently tailored to tabletop manipulation [126, 34, 116, 74, 20, 52, 91, 63, 66]. As a result, current datasets do not support a unified set of tasks spanning motion capture, egocentric multimodal perception, action understanding, and interaction modeling with rich scene context. This gap has become a major bottleneck for advancing data-hungry models in human motion understanding, behavior analysis, and embodied AI.

Among existing efforts, the Nymeria dataset [93] is an attractive resource. Captured with Project Aria [48] glasses and Aria-like wristbands, it records more than 300 hours of in-the-wild human activities and provides annotations including body motion, device trajectories, synchronization, semi-dense point clouds, and in-context narrations. However, the released body motion is primarily optimized for spatial alignment with the glasses, without explicitly addressing artifacts introduced by inertial MoCap. In addition, the dataset relies on a human model that is not widely adopted in academia, limiting interoperability with existing benchmarks. Finally, the semi-dense point clouds are often insufficient for algorithms that require semantic and geometric scene context. To address these limitations, we upgrade Nymeria and introduce NymeriaPlus. NymeriaPlus substantially extends the original dataset along four dimensions. First, it provides improved body motion annotations, increasing the accuracy and robustness of estimated body shape and pose. We release results in two widely used, open-source parametric human models: Momentum Human Rig (MHR) [50] and SMPL [87, 88]. Second, we add 3D and 2D bounding box annotations for all indoor recordings to support scene-aware motion understanding. Using a closed-set taxonomy of 19 common categories, we label more than 10K unique object instances, spanning both movable objects (e.g., tables, chairs, storage units, and lamps) and structural elements (e.g., walls, floors, and stairs). We further complement these annotations with an open-set taxonomy in selected scenes, labeling an additional 10K unique objects to capture richer semantic context. Third, we introduce densely populated, spatially grounded 3D object reconstructions, facilitating fine-grained interaction-aware motion understanding and embodied reasoning. Finally, NymeriaPlus releases additional modalities excluded from prior releases, including dedicated scans of each indoor location that capture complete static scene geometry, as well as auxiliary sensor streams (e.g., wristband videos, headset audio, and calibration data).

By combining accurate 3D human motion with dense object annotations at scale, NymeriaPlus bridges the gap between in-the-wild egocentric perception, rich scene context, and human motion that has constrained prior datasets. We expect this release to enable a broad range of tasks, including environment-aware motion tracking and synthesis, action and interaction understanding, object detection, 3D reconstruction, and multimodal learning for embodied contextual AI.

## 2 Related Works

**Egocentric Multimodal Datasets.** Egocentric datasets have been developed for over a decade. Early efforts such as EgoHands [19], EGTEA [82], EPIC-KITCHENS [39, 40], EgoCom [103], H2O [78], DexYCB [34], and Assembly101 [116] primarily comprise small-scale collections recorded with head-mounted cameras or AR/VR headsets, and focus on hand–object interactions and activity understanding. Ego4D [55] was the first large-scale in-the-wild egocentric dataset, capturing diverse daily activities using wearable glasses and

leveraging human narrations as a key annotation signal. More recently, the growing availability of AR/VR headsets [4, 2, 6, 1] and smart glasses [7, 48, 5] has led to a rapid expansion of multimodal egocentric datasets. For instance, HoloAssist [134] provides 166+ hours of paired performer–instructor recordings to support interactive assistant research. EgoExo4D [56] captures 180+ hours across eight skill categories to study skilled activities. Nymeria [93] records 300+ hours of daily activities for understanding egocentric body motion. EgoLife [140] introduces a long-horizon question answering benchmark by collecting 266+ hours of footage from six people living in an apartment for a week. LaMAria [77] captures more than 22 hours of ground-truth device localization to benchmark SLAM. DTC [45] collects 2,000+ 3D object scans to benchmark object reconstruction. EgoDex [63] records 800+ hours of table-top hand–object manipulation. Reading-in-the-Wild [138] records 100+ hours with ground-truth gaze for recognizing reading activities. UniHand2.0 [92] collects 35K+ hours of egocentric human demonstrations for robot learning. In addition to these large-scale efforts, numerous smaller datasets have been proposed [58, 145, 11, 72, 104, 73, 150, 20, 148, 28, 69]. Despite this progress, there remains a lack of datasets that consolidate comprehensive annotations within a single corpus, which limits research on cross-modality reasoning. NymeriaPlus addresses this gap by augmenting the open-sourced Nymeria dataset with accurate parametric human motion, 3D object bounding boxes, and 3D object reconstruction, thereby enriching its existing multimodal sensing, multi-device localization, synchronization, and in-context narration.

**Human Motion Datasets.** Human motion datasets have a long history, spanning both laboratory motion capture and in-the-wild recordings. A prominent effort is AMASS [94], which aggregates numerous MoCap datasets [9, 61, 54, 128, 31, 14, 26, 90, 126, 27, 102, 35, 119, 95, 96, 76, 127, 89, 89, 12, 53, 130, 64, 129, 83] into a unified SMPL-(X) representation [87, 88, 107], enabling large-scale analysis and learning. While AMASS offers high-fidelity and diverse motion, it lacks environmental and interaction context. Recent datasets therefore incorporate object motion and human–object interactions [104, 13, 74, 67, 91]. Beyond MoCap, RGB-(D) cameras are widely used to capture motion, either from monocular videos [117, 114, 57, 30, 141, 84, 21, 49, 125, 135] or multiview systems [68, 145, 72, 73, 56, 91, 98]. For monocular capture, Motion-X [84, 147] and MotionMillion [49] are notable for their scale, leveraging large collections of internet video. For multiview capture, EgoExo4D [56] and Embody3D [98] represent two large-scale efforts. However, monocular approaches are poorly suited to egocentric viewpoints due to limited visibility of the body, and multiview systems typically trade off scene realism and activity coverage. To enable in-the-wild motion capture, wearable MoCap suits have emerged as a practical alternative [129, 131, 58, 70, 71, 139, 80, 93]. To mitigate artifacts inherent to non-vision-based tracking, prior work combines IMUs with vision [129, 131], constrains motion locally [139], or optimizes motion using 3D scene context [58, 80] or egocentric headset tracking [93]. Among these, Nymeria is a particularly large-scale in-the-wild egocentric collection, yet it still exhibits notable motion artifacts. Only a subset of motion datasets explicitly targets egocentric capture [58, 145, 104, 72, 73, 56, 93, 108]. In such settings, scene context is often represented either via dense reconstructions [145] or point clouds [58, 56, 93]. While ADT [104] and HD-EPIC [108] provide semantic object context, their scene diversity remains limited. Simulation can further scale data collection [11, 25, 67, 13, 81], but synthetic data often suffers from domain gaps due to imperfect noise and appearance models.

**Semantic Bounding Box Datasets.** 3D bounding box benchmarks vary widely in (i) the underlying sensing modality and data format, (ii) dataset scale, and (iii) the granularity and taxonomy of annotated object categories. Traditional benchmarks include single-frame RGB-D datasets such as SUN RGB-D [120], large-scale room-scanning datasets such as ScanNet [38, 142] and ARKitScenes [23], and object-centric scanning datasets such as Objectron [10] and CO3D [112]. Omni3D [29] further unifies several of these sources (along with autonomous driving and simulation datasets) to train single-view 3D object detectors that generalize across domains. With the emergence of egocentric video, several smaller-scale 3D bounding box datasets have also been introduced. Notably, AEO [124] provides a diverse evaluation set for egocentric 3D object detection, while ADT [104] offers 3D box annotations in a single-room environment. The large performance gap observed when applying scanning-dataset-trained 3D detectors to AEO motivates the release of NymeriaPlus. In analogy to recent trends in 2D detection, a key direction in 3D detection is open-set, category-agnostic localization. CA-1M [79] advances this goal by adding open-set 3D bounding boxes to ARKitScenes. Complementarily, NymeriaPlus provides 12k open-set 3D bounding boxes for training and five scenes with exhaustive 3D OBB annotations for validation.

**Object Reconstruction Datasets.** While numerous datasets have driven recent progress in 3D vision, they

typically force a trade-off between detailed object geometry and natural environment context. Existing 3D datasets largely focus on isolated objects (e.g., ShapeNet [33], Objaverse [43, 42], ABO [36], GSO [46], DTU [8], uCO3D [86]), which inherently lack the realistic clutter, lighting, and occlusions of natural environments. Conversely, real-world scene datasets (e.g., ScanNet [37], ScanNet++ [143], Matterport3D [32], Replica [123]) capture natural context but represent scenes as monolithic meshes, resulting in incomplete geometry, limited per-object resolution, and an inability to cleanly separate instances from their surroundings. Synthetic scene datasets (e.g., Hypersim [113], 3D-FRONT [51], SceneSmith [109], Aria Synthetic Environments [17]) provide perfect instance separation but suffer from a well-documented sim-to-real gap due to simplistic layouts and an absence of natural physical clutter. Other approaches attempt to populate real scene scans by retrieving and aligning CAD assets (e.g., Scan2CAD [15], ScanNotate [110], Metascenes [144], LiteReality [65]); however, these CAD models serve only as approximate proxies and fail to capture the exact, fine-grained geometric shape of the actual objects. While a few datasets do capture exact real objects within real scenes, they are heavily constrained in scale: the ShapeR [118] evaluation set consists of only 7 sparsely annotated recordings, and Aria Digital Twin [105] is restricted to two scenes. In contrast, our dataset provides dense, instance-level real 3D geometry for objects situated naturally in real-world scenes across 47 distinct recordings, effectively bridging the gap between isolated object geometry and complex scene context.

### 3 NymeriaPlus Dataset

#### 3.1 Recap of Nymeria Dataset

In this section, we briefly recap the Nymeria dataset [93]. Nymeria comprises more than 300 hours of in-the-wild human activities recorded from 256 participants across 50 indoor and outdoor locations and 20 unscripted scenarios. Each participant wore Project Aria glasses [48] and two Aria-like wristbands (miniAria), which record RGB, grayscale, and eye-tracking videos, IMU measurements, barometric pressure, and audio. Participants also wore an XSens MoCap suit [101] that captures full-body kinematics at 240 Hz. In each recording session, an observer wearing Project Aria glasses captured third-person views of the participant. All devices are time-synchronized and localized in a shared metric 3D coordinate system. The original release provides annotations including 6-DoF device trajectories, semi-dense point clouds, gaze, XSens kinematic motion, and retargeted parametric body motion produced using the Meta Momentum library [100]. It also includes human narrations at three levels of granularity (motion narration, atomic actions, and activity summaries). Since release, Nymeria has supported a range of research directions, including motion tracking and generation [59, 62], activity understanding [62, 132, 106], video generation [18, 136], and dynamic reconstruction [137].

Despite its scale and rich multimodal sensing, the original Nymeria dataset has several limitations that motivate the extensions introduced in NymeriaPlus. First, the provided human motion is obtained via a naïve optimization that aligns the XSens motion with the Aria world frame, but does not explicitly address motion artifacts. In practice, the most prominent errors occur at the end effectors, manifesting as inaccurate wrist positions and noticeable foot sliding. Second, environmental context is represented as a semi-dense point cloud reconstructed via VIO/SLAM, which lacks both semantic understanding and dense surface geometry. This limits the ability to reason about human motion under scene constraints, where semantics and detailed surfaces are often essential. In the remainder of this section, we summarize the key components of NymeriaPlus: Sec. 3.2 describes our motion optimization pipeline, Sec. 3.3 presents the 3D/2D bounding box annotations, Sec. 3.4 introduces object shape reconstructions, and Sec. 3.5 details the additional modalities and recordings released with the dataset.

#### 3.2 Body Motion Optimization

We provide ground-truth 3D human motion for the entire dataset by formulating an optimization framework that leverages both XSens and Aria streams. While Nymeria [93] retargets XSens motion to an anatomically inspired human model to obtain 3D motion, we identify and address three key limitations of that approach. First, it uses a proprietary human model, limiting compatibility with widely adopted parametric body representations. Second, it retargets XSens motion to the body model using an artist-defined skeleton mapping, which can be brittle under XSens calibration errors or out-of-distribution body shapes (e.g., very

short or tall subjects), yielding implausible bone lengths. Third, it does not leverage Aria streams during optimization; instead, it aligns the XSens-retargeted motion to the metric Aria 3D world in a post-processing step. This can introduce artifacts such as arm–torso self-penetration (due to lower end-effector accuracy in inertial MoCap), temporal jitter, and foot sliding (due to per-frame mapping errors from the XSens frame to the Aria world). In the following sections, we address each of the points above in more detail by introducing the body model used in NymeriaPlus (Sec. 3.2.1) and the optimization framework combining XSens and Aria streams (Sec. 3.2.2). To ensure compatibility with other human motion datasets proposed in the literature, we also provide all NymeriaPlus motions in the SMPL(-X) body model parameterization [87, 107], leveraging an ad-hoc retargeting approach (Sec. 3.2.3).

### 3.2.1 MHR Human Model

We build our framework on the recently released Momentum Human Rig (MHR) model [50]. MHR is a parametric human body model defined as a function  $M(\beta, \theta)$  that outputs a 3D mesh with  $N$  vertices. It takes as input shape parameters  $\beta$  (coefficients of a linear identity space) and skeletal parameters  $\theta \in \mathbb{R}^{204}$ . The parameter vector  $\theta$  controls a 127-joint skeleton and can be decomposed into 136 pose parameters, which specify joint angles, and 68 identity parameters, which capture subject-specific bone lengths. We denote these components as  $\theta^P \in \mathbb{R}^{136}$  and  $\theta^I \in \mathbb{R}^{68}$ , respectively. We further denote by  $J(\theta) \in \mathbb{R}^{127 \times (4 \times 4)}$  the per-joint affine transformations induced by  $\theta$ . Given  $J(\theta)$ , mesh vertices are computed via linear blend skinning (LBS).

Since XSens does not provide reliable body-shape information, we omit  $\beta$  from our optimization. We instead model per-frame pose using  $\theta^P$  and per-subject skeletal identity (i.e., bone-length parameters) using  $\theta^I$ . This choice leverages a key property of MHR: unlike SMPL(-X) [87, 107], it decouples the body surface from the underlying skeleton, enabling fine-grained control over bone-length proportions.

### 3.2.2 Motion Optimization with MHR

As in Nymeria, we use XSens software [101] to preprocess skeletal motion and Project Aria MPS [48] to localize the Aria glasses and miniAria wristbands in a shared metric 3D world. In Nymeria, XSens motion is retargeted to the body model and then rigidly transformed from the XSens coordinate frame to the Aria world via hand–eye calibration [121], without leveraging miniAria tracking signals or environmental context during optimization. In contrast, we (i) regress subject-specific bone lengths to obtain robust identity estimates, (ii) use these estimates to improve retargeting, and (iii) jointly optimize MHR against the XSens-retargeted motion and Aria trajectories in the metric 3D world.

**Bone length regression.** We observe that XSens skeletons can exhibit inaccurate body proportions. To mitigate this issue, we train a regressor that takes the subject-reported height as input and predicts MHR identity parameters  $\theta^I$ . We use ridge regression with leave-one-out cross-validation and leverage the training set introduced in [50], which contains 7,110 scans registered to the MHR model. Although the regressor does not account for small height discrepancies due to footwear or hairstyle, we found it to be robust in practice.

**XSens motion retargeting.** We obtain an initial motion estimate by retargeting XSens motion to MHR. Our method solves an inverse-kinematics optimization similar to [93]: given 23 XSens skeleton segments and 79 anatomical landmarks, along with an artist-designed mapping to the MHR skeleton, we estimate per-frame pose parameters  $\theta^P$  and per-subject identity parameters  $\theta^I$ . During optimization, we strongly regularize  $\theta^I$  toward the identity predicted by our regressor. While the resulting motion sequence  $\Theta^X$  is generally plausible, it is computed in the dead-reckoned XSens trajectory and therefore suffers from drift. Moreover, as is common in inertial motion capture, errors accumulate along the kinematic chain, leading to wrist pose inaccuracies and occasional self-penetrations between the arms and torso.

**Joint XSens–Aria optimization.** To reduce drift and kinematic inaccuracies from the previous stage, we leverage Aria and wristband 6-DoF trajectories and formulate a joint XSens–Aria optimization framework. This setting introduces several practical challenges. First, XSens and Aria trajectories lie in distinct coordinate frames (sharing only the gravity direction); XSens global trajectory drifts over time, making the transformation aligning XSens and Aria world coordinates unknown and varying over time. Residual misalignment can then introduce inconsistencies between global and local motion, for example in the form of foot sliding. Second, the placement of the Aria glasses and wristbands on the subject is only known up to calibration error and may

vary slightly over time. Third, we cannot rely on accurate foot-ground contact information: floor annotations (Sec. 3.3) are accurate only up to a 1-2 centimeter for indoor scenes and are unavailable outdoors; while XSens provides contact labels, we find them unreliable especially when subjects climb up stairs and transition across floors.

Our optimization framework takes as input retargeted motion  $\Theta^X$  and Aria head trajectories  $T^H$  plus wristband trajectories  $T^{Wr}$  over a sequence. It outputs motion  $\Theta^W$  in Aria world coordinates. First, we seek a sequence of frame-varying transformations roughly aligning XSens and Aria coordinate frames. As in [93], we assume a constant transformation  $T_{X \rightarrow D}$  from the XSens head segment to the Aria device D and estimate its value via HandEye calibration [121]. Combining  $T_{X \rightarrow D}$  with  $T^H$ , we obtain a sequence of per-frame rigid transformations converting motion  $\Theta^X$  into Aria world,  $\Theta^{W,rigid}$ . Note that this is exactly the post-processing step used in [93]. While the approach can provide a preliminary alignment, it is not robust to inaccuracies in  $T_{X \rightarrow D}$ , in  $T^H$ , and in  $\Theta^X$  (especially around the neck area).  $\Theta^{W,rigid}$  exhibits temporal jitter and pose inaccuracies accumulating along the kinematic chain, particularly visible as foot sliding artifacts.

Taking  $\Theta^{W,rigid}$  as initialization, we define an optimization problem seeking a refined motion  $\Theta^W$  in the Aria coordinate frame. Namely, we minimize the following objective function:

$$\begin{aligned} \mathcal{L}(\Theta^W) = & \mathcal{L}_T(\Theta^W; T^H, T^{Wr}) + \lambda_X \mathcal{L}_X(\Theta^W; \Theta^X) + \lambda_l \mathcal{L}_l(\Theta^W) + \lambda_{smooth} \mathcal{L}_{smooth}(\Theta_{root}^W) \\ & + \lambda_g \mathcal{L}_g(\Theta^W; \Theta^X) + \lambda_f(w_{vel}) \mathcal{L}_f(\Theta^W; \Theta^X) \end{aligned} \quad (1)$$

where  $\mathcal{L}_T$  is a robust loss penalizing position errors between MHR head and wrist joints and Aria trajectories,  $\mathcal{L}_X$  enforces local joint angles to be similar to the ones retargeted from XSens,  $\mathcal{L}_l$  enforces pre-defined limits on model parameters,  $\mathcal{L}_{smooth}$  enforces temporal smoothness on the body root global translation and rotation, and  $\mathcal{L}_g$  encourages similar body root joint orientation along the gravity direction between  $\Theta^W$  and  $\Theta^X$ . To mitigate foot sliding,  $\mathcal{L}_f$  enforces constant position for MHR foot joints in frames where feet are deemed in contact (when XSens foot contact labels are available) or where XSens foot velocities  $vel_X$  are close to 0 (velocity norms computed from  $\Theta^X$ , when contact labels are not available). To avoid motion discontinuities, for  $\mathcal{L}_f$  we adopt an adaptive weighting schema defining  $\lambda_f(w_{vel}) = \lambda_0 + \lambda_\alpha e^{-vel_X/v_\sigma}$ , where  $\lambda_0$ ,  $\lambda_\alpha$ ,  $v_\sigma$  are fixed hyperparameters; for frames in which feet are in contact, we set  $vel_X$  to 0. The other  $\lambda$  values in Eq. (1) weight the contributions of the different error terms.

We minimize the objective in Eq. (1) sequentially, over batches of 2000 frames, with an efficient Gauss-Newton solver, using the python API from the Momentum library [100].

### 3.2.3 MHR to SMPL Conversion

To maximize interoperability with existing datasets and models, we additionally release all ground-truth motions in the SMPL(-X) [87, 107] parameterization. We perform this conversion using the open-source SMPL-to-MHR tool released with MHR [50]. For completeness, we briefly outline the procedure.

We first define an artist-curated correspondence between MHR and SMPL templates. Concretely, we warp the SMPL template to match the MHR template geometry and associate each SMPL vertex with a surface point on the MHR template via triangle identifier and barycentric coordinates. This correspondence enables converting an MHR mesh to the SMPL topology via barycentric interpolation.

Given an MHR motion sequence, we re-topologize each resulting MHR mesh to the SMPL topology and then solve an optimization problem to recover the corresponding SMPL parameters. Specifically, given a sequence of MHR meshes  $M^{\text{MHR}}$  (re-topologized to SMPL), we optimize for the SMPL parameters  $\Psi$  (including shape and pose) by minimizing the following objective:

$$\mathcal{L}(\Psi) = \mathcal{L}_V(\Psi; M^{\text{MHR}}) + \lambda_E \mathcal{L}_E(\Psi; M^{\text{MHR}}) \quad (2)$$

where  $\mathcal{L}_V$  penalizes the Euclidean distance between optimized SMPL vertices  $M(\Psi)$  and target (re-topologized) MHR vertices and  $\mathcal{L}_E = \sum_{(v,v') \in \varepsilon} \|(M(\Psi)_v - M(\Psi)_{v'}) - (M_v^{\text{MHR}} - M_{v'}^{\text{MHR}})\|$  penalizes edge discrepancies, over the set of SMPL template edges  $\varepsilon$ , with an  $L1$  loss.  $\lambda_E$  balances the contribution of the two terms.

Given the problem is highly non-convex, optimization proceeds in multiple stages to avoid getting stuck in local minima. First, we optimize a set of identity parameters over a set of sparse frames, selected based on a

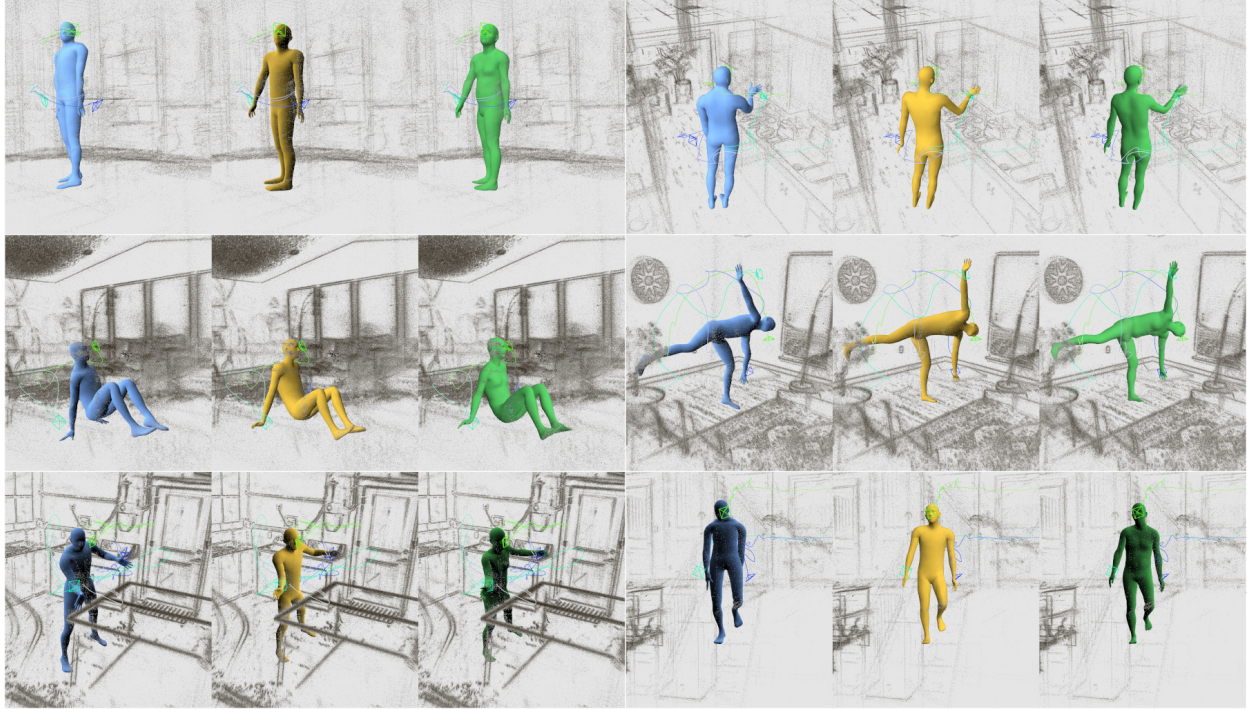


**Figure 1 Nymeria and NymeriaPlus motion samples.** We compare Nymeria results (blue) against the new MHR (yellow) and SMPL (green) ones. Each frame also shows Aria head and wrist trajectories. NymeriaPlus results exhibit more realistic body proportions and better matching of wrist trajectories, resulting in fewer body self-penetrations and improved placement with respect to the 3D scene.

given heuristic (e.g., pose diversity or geometric similarity with the rest template). Then, we optimize for body pose and refine identity by minimizing the loss in Eq. (2) according to a hierarchical scheme, fitting first global orientation and then all parameters simultaneously. At each stage, we rely on the Adam optimizer provided by the pytorch library [3].

### 3.2.4 Metrics and Evaluations

We evaluate the quality of the MHR ground-truth motions by comparing them against the original Nymeria ones. Based on metrics results, we identify and filter out 17 problematic sequences from the original dataset – mostly due to wrist recording issues. In total, NymeriaPlus collects 1083 sequences.

We consider three metrics:

- **Wrist distance error:** We compute the distance (in cm) between the body model wrist joints and the miniAria wristband positions, per frame. Note that this error includes a constant offset (from the wrist joint to the wristband coordinate frame origin), which is however the same across models and thus ensures a fair comparison.
- **Body self-penetration error:** We leverage the collision error term implemented in the Momentum library [100]. It approximates the body as a set of geometric primitives and detects their collision, by iterating over pairs of primitives and checking if they overlap; overlap is determined by comparing their positions, directions, and radii. This collision detection routine is available for both MHR and the body model used in Nymeria.
- **Foot sliding error:** We consider the frames in which XSens detects foot contact, and compute the body model foot joint velocities in these frames. Following previous work [146], we consider foot sliding occurs if joint velocity exceeds 10cm/s during contact; we then compute the percentage of (contact) frames in which sliding is detected. We limit the computation to the heel joint since we find its contact more

reliably detected by the XSens software.

For each metric, we compute an average error over all the NymeriaPlus sequences after downsampling them to 30 fps. We also show visual results in Fig. 1, comparing Nymeria results (blue) versus the new motions in MHR (yellow) and SMPL (green) format.

As for wrist distance, the average error computed on the original Nymeria dataset is 14.32cm, which decreases to 5.07cm for NymeriaPlus (please recall that this error also includes the offset between miniAria and wrist joint). Numbers are well reflected by visual results, showing how the body model wrists now better match miniAria trajectories. A similar trend is confirmed by the body self-penetration error, whose average is 18.67 in Nymeria and 2.44 in NymeriaPlus. In particular, self-penetration between arms and torso was problematic in Nymeria given its reliance on XSens motions only. By leveraging both XSens and Aria trajectories at optimization time, we are able to significantly reduce these artifacts in NymeriaPlus.

Mitigating foot sliding proved challenging. The difficulty lies in the absence of reliable foot contact labels and of strong input signals for the lower-body motion (in Aria world, we can just rely on head and wrist streams, leaving the problem of reconstructing lower-body motion less constrained). Nonetheless, we show improvement going from 35% frames deemed as “exhibit foot sliding” in Nymeria down to 9.81% in NymeriaPlus.

### 3.3 Bounding Box Annotations

We annotate all NymeriaPlus recordings with 3D oriented bounding boxes (OBBs) and their corresponding 2D projections to facilitate object-level 3D grounding and scene-aware motion reasoning. We describe both our fixed-taxonomy and open-set 3D OBB annotation pipelines. At a high level, we first collect dedicated “basemap” recordings for each indoor venue and annotate them with 3D boxes. We then transfer these basemap annotations to each Nymeria recording by exploiting the shared coordinate system provided by localization. Since objects may move across sessions, annotators subsequently verify and refine the transferred boxes and add sparse open-set OBB annotations. Finally, we exhaustively annotate five basemaps using an open-set taxonomy to enable benchmarking of open-set 3D OBB detectors. We provide detailed statistics and qualitative visualizations for the resulting 3D object annotations in the NymeriaPlus release.

#### 3.3.1 3D Annotation Tool

We developed a 3D OBB annotation tool, Boxy (Fig. 2). Boxy takes as input the original video, online-estimated camera intrinsics, optimized 6-DoF device trajectories, and the semi-dense point cloud. Annotators place 3D OBBs around static objects and adjust their 9-DoF directly in 3D, using both the point cloud and the projected box overlays in the image for guidance and verification. To facilitate annotation, Boxy can automatically select informative multi-view frames based on the observability of the semi-dense point cloud.

#### 3.3.2 2D Bounding Box

For 3D OBB detection – both single-view methods such as Cube R-CNN [29] and multi-view methods such as EVL [124] – it is important to know which 3D boxes are visible from a given viewpoint and the corresponding 2D bounding boxes (2DBBs) they induce. Manually annotating per-frame 2DBBs and visibility is prohibitively expensive due to the large number of views per object; we therefore compute these quantities automatically. To estimate visibility, we require that (i) the 3D OBB projects into the image, (ii) at least two semi-dense points fall inside the 3D box, and (iii) at least 85% of the projected 3D box lies within the valid image region. We compute the associated 2DBB by projecting the 3D box into the image and taking the axis-aligned bounding box enclosing samples along its edges. This automated procedure is not error-free and can introduce occasional temporal flicker when visualizing projected boxes. Nevertheless, we found the resulting annotations to be sufficient for training and evaluating 3D OBB detectors, and we leave further temporal smoothing and refinement to future work.

#### 3.3.3 Basemaps and 3D Annotation Transfer

**Basemaps.** Nymeria contains 1,100 sequences recorded across 50 locations, including 47 indoor house venues. Annotating every recording independently would require substantial manual effort. We therefore exploit the



**Figure 2 Boxy 3D OBB annotation tool interface.** (Left) The 3D point cloud and a 3D gizmo are used to modify all nine degrees of freedom of the box directly in 3D. (Right) The current 3D box annotation is projected into the RGB image. Annotators can iterate across views to inspect alignment.

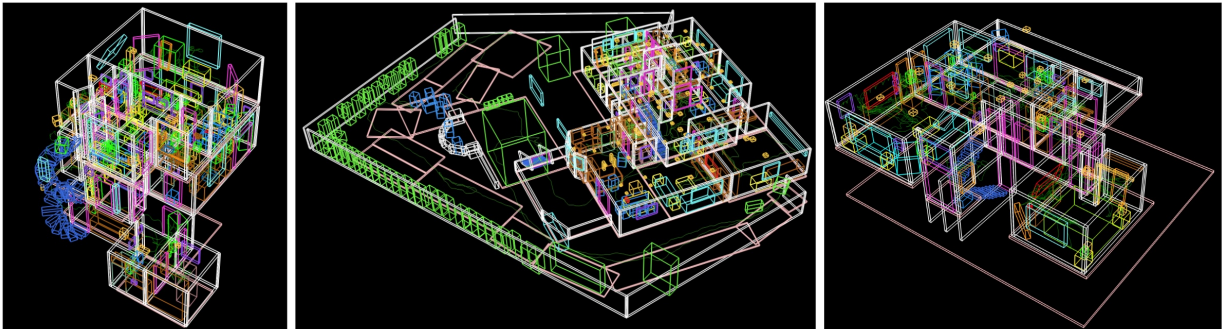


**Figure 3 Basemap 3D OBB annotations.** We visualize basemap annotations for three venues from NymeriaPlus.

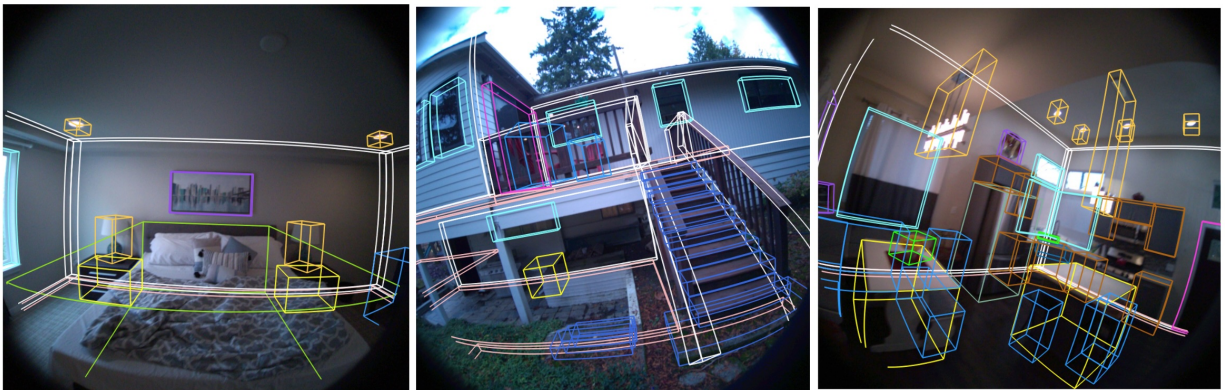


**Figure 4 Basemap 2D OBB annotations.** Visible 3D OBBs from three venues are rendered into sample RGB frames.

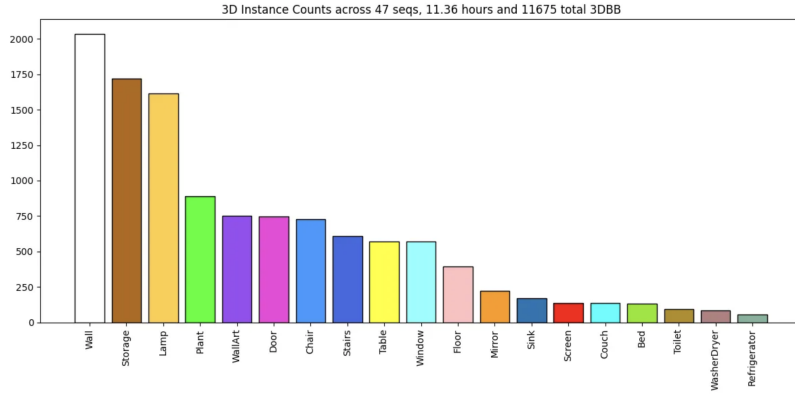


**Figure 5 Basemap unique 3D objects histogram.** We count the number of unique 3D OBBs across the basemaps for each class. Since we transfer these OBBs to the individual scenario recordings, this is the fundamental distribution over observed objects. Note that transferring the OBBs to scenario recordings increases the viewpoint diversity substantially over just the basemap sequences.



**Figure 6 Example sparse open-world annotations.** (left) A fixed taxonomy of objects and structure are first annotated. (middle) Additional "anything" objects are added, roughly 12 per recording. (right) All objects visualized together.

fact that Nymeria localizes all recordings captured at the same venue within a shared coordinate system. Since recordings at a given venue are always collected within 2–4 consecutive days, the environment tends to remain largely static. During Nymeria data collection, most indoor venues were scanned using a single pair of Project Aria glasses to create dedicated “*Basemap*” recordings. These basemaps are designed to observe the full 3D space from diverse viewpoints, where operators were instructed not to modify or interact with the scene to preserve its static layout. When a venue does not include a basemap, we manually select one of the existing recordings that covers the space well while exhibiting minimal human–scene interaction (five basemaps from *Welcome To My Home* and three from *Scavenger Hunt*). In total, we collected 47 basemap recordings, one per indoor house venue, each typically 5–15 minutes long. Fig. 3 visualizes 3D OBB annotations for three venues, and Fig. 4 shows their projections onto RGB frames.

**Annotation transfer and refinement.** After annotating the basemaps, we transfer their boxes to all recordings captured at the same location using the shared coordinate frame, and then refine each 3D OBB. Because most objects are static (*e.g.*, walls, floors, cabinets, and dressers), this refinement is relatively lightweight. Annotators remove boxes for objects that are no longer present or not observed in the target recording, and adjust boxes for objects that have been slightly moved. We note that some recordings may capture previously unseen rooms or areas; in such cases, newly observed objects may not have corresponding annotations.

### 3.3.4 Fixed Set Taxonomy

We adopt 19 commonly occurring object categories to define a closed-set taxonomy for 3D OBBs. This taxonomy is similar to the classes used in EFM3D [124] (see Sec. A for detailed definitions). In addition to common objects (*e.g.*, beds, chairs, lamps, and tables), our taxonomy includes structural classes such as floors, walls, and stairs, which are informative for scene-aware motion reasoning.

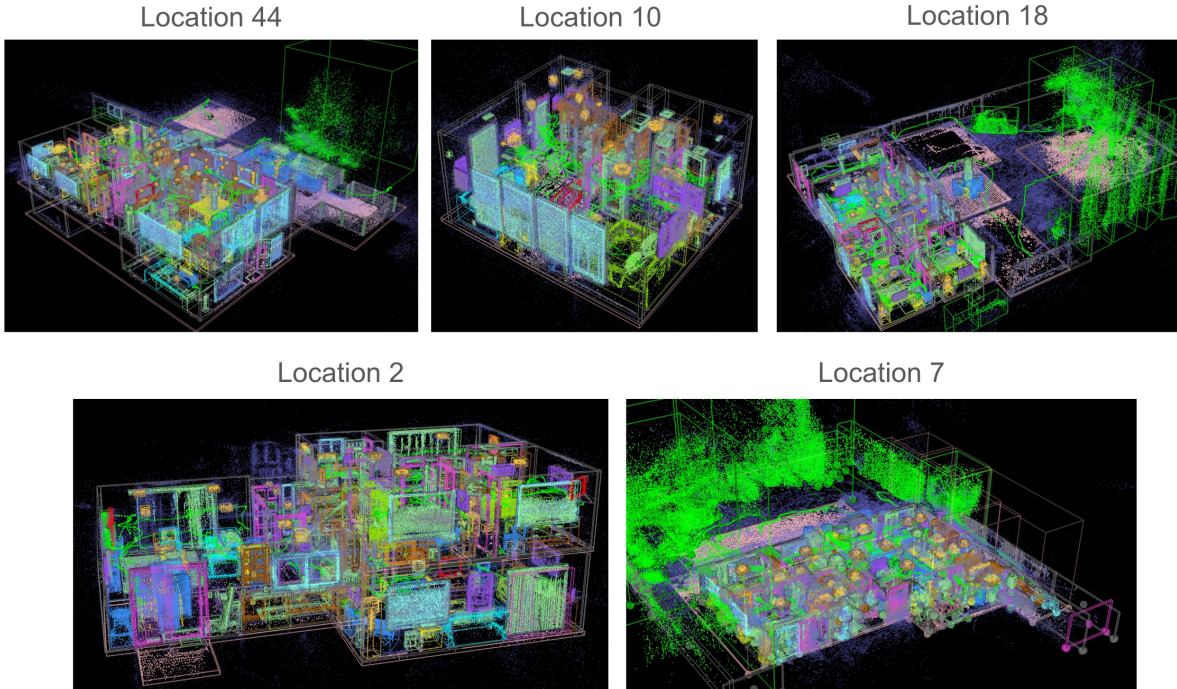


**Figure 7** **Densely annotated venues.** We annotated five static basemaps densely with "every" object annotated.

### 3.3.5 Open Set Taxonomy

**Sparse open set annotations.** We further augment each recording with a set of *Anything* objects, capturing instances that fall outside the fixed taxonomy. These annotations often correspond to objects that are frequently moved (e.g., cups, bags, and bottles). Because Boxy does not currently support dynamic-object annotation, we do not label *Anything* objects on basemaps; instead, we annotate a sparse set independently for each recording. On average, we annotate 12 *Anything* objects per recording. As this process is intentionally non-exhaustive due to annotation cost, the resulting labels provide broad coverage of long-tail objects without requiring complete scene annotation. Overall, we collect approximately 12K *Anything* object annotations across NymeriaPlus, which is comparable in scale to the fixed-taxonomy 3D OBB annotations. Fig. 6 shows a qualitative example.

**Dense open set with captions.** For five basemaps, we provide exhaustive open-set annotations to serve as an evaluation set for open-world 3D OBB detection (Fig. 7). While the notion of an “object” can be subjective, we aim to annotate the scenes as densely as possible. We prioritize objects that are movable or that correspond to interactive parts (e.g., handles, knobs, and switches), and we omit fine-scale textures and highly non-cuboidal structures (e.g., cables), as well as low-level structural elements such as individual floor tiles. Across the five densely annotated venues, we label a total of 2,896 objects (579 per venue on average). In addition, annotators provide a short descriptive caption for each object (adjective + noun) to facilitate identification within the scene (e.g., “cabinet handle” or “red velvet curtain”). Fig. 8 shows examples of these dense annotations with captions.

## 3.4 Object Reconstruction with ShapeR

To provide a more detailed geometric representation beyond coarse spatial bounds, we also release dense metric 3D shape reconstructions inferred via ShapeR [118] for a subset of the 3D bounding boxes (Figure 10). Specifically, we exclude basic structural elements (e.g., walls, floors, ceilings, doors, stairs, and windows) whose geometry is already well-approximated by their bounding volumes. For the remaining object categories, we leverage the probabilistic nature of ShapeR to generate four candidate meshes per instance. To ensure high geometric fidelity, these proposals undergo a rigorous manual quality control process. Human annotators



**Figure 8 Example dense annotations.** Examples of dense, open-world annotation are shown with the corresponding text caption.

evaluate and rate the candidate reconstructions via a dedicated web interface. In the final dataset, we release the single highest-rated mesh for each bounding box, provided it meets a quality threshold. In the remainder of this section, we detail the inference procedure used to generate these candidates and outline our manual quality-control protocol.

### 3.4.1 Candidate Reconstruction Generation

ShapeR [118] requires the following instance-specific inputs for reconstruction: a semi-dense point cloud, multiple posed images, and a text description. We process the NymeriaPlus sequences to extract these inputs for each 3D bounding box. Because a bounding box encompasses all spatial geometry within its limits, a naive point extraction often includes background clutter or parts of adjacent objects (e.g., table points captured within a chair’s bounding box). To isolate the target geometry, we project the enclosed 3D points into the 2D camera frames and apply SAM2 [111] masks to filter out non-instance points, resulting in a clean, object-centric point cloud.

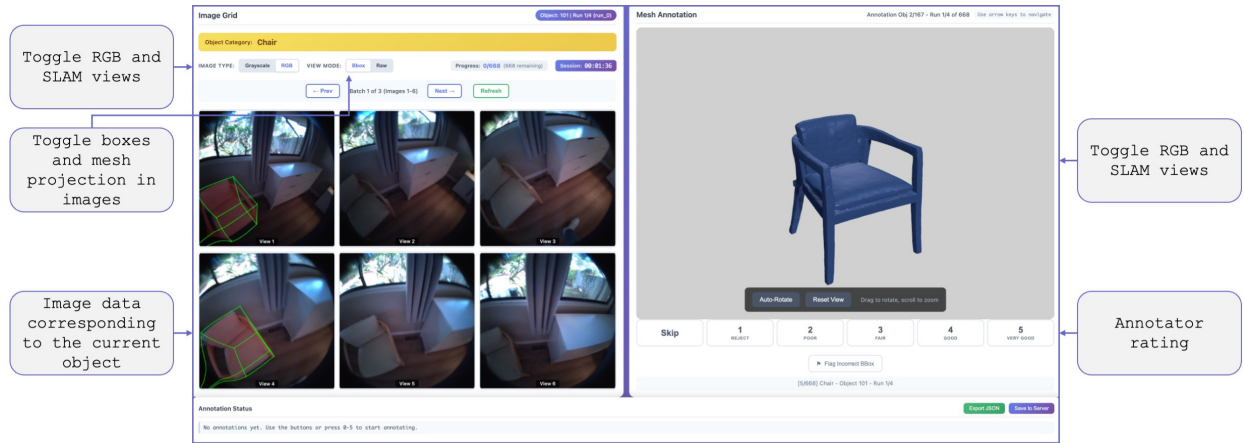
Using the visibility associations between these filtered 3D instance points and the 2D frames, we identify all images where the object is visible. From this set, we sample 16 frames using a greedy view-selection heuristic designed to maximize viewpoint diversity and image quality. To generate the required text conditioning, we pass 4 of these selected views to a Vision-Language Model (VLM) [99] to obtain a descriptive shape prompt.

Finally, the 16 posed views, the filtered instance point cloud, and the VLM-generated text description are passed to ShapeR. Because the underlying flow-matching formulation is probabilistic and can yield variations in geometric fidelity, we run inference 4 times per object. This produces a set of four distinct metric candidate meshes per instance, ensuring we can subsequently select the highest-quality shape during the manual annotation phase.

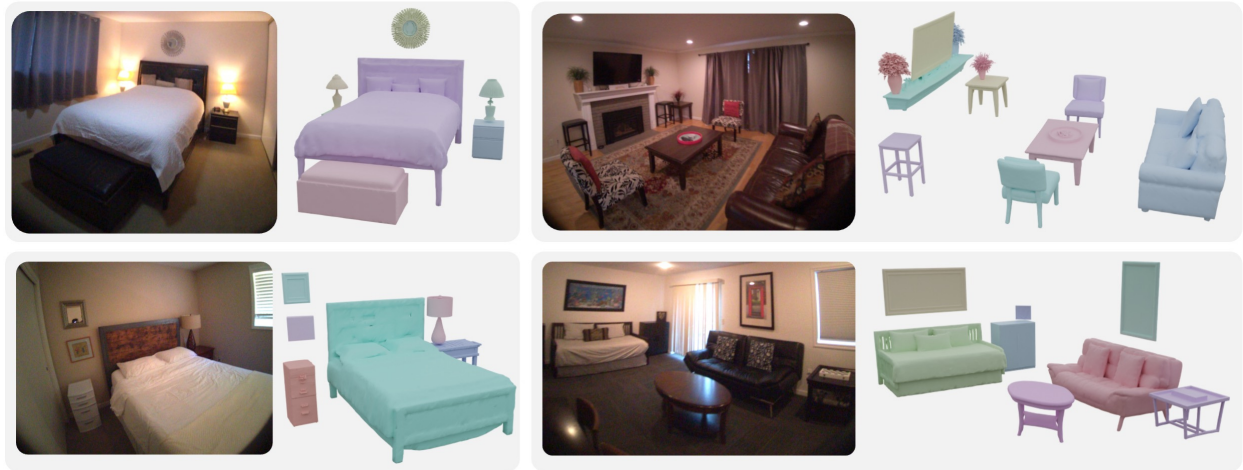
### 3.4.2 Annotation Process

Figure 9 illustrates our custom annotation interface, designed to manually verify the fidelity of the ShapeR-generated 3D meshes. For a given bounding box, the interface displays the corresponding multi-view RGB images, grayscale images and relevant metadata such as the object category. To aid alignment verification, annotators can toggle 2D rendering of both the bounding box and the candidate mesh. An interactive 3D viewer on the right side of the screen allows users to inspect the generated mesh from arbitrary viewpoints. Using these visual references, annotators evaluate the reconstruction quality on a scale from 1 (poor) to 5 (excellent). This rating process is conducted for all four ShapeR candidate predictions per bounding box. We retain only the single highest-rated mesh for each instance, while strictly requiring a minimum quality score of 3 to be included in release.

Our dataset-wide annotation pipeline is executed in three distinct phases. In the first phase, we exhaustively evaluate candidate meshes for the 47 basemap recordings, obtaining valid, high-quality shapes for 4547 out of



**Figure 9 Shape Annotation Interface.** Our custom tool for verifying ShapeR-generated meshes. Annotators inspect an interactive 3D reconstruction (right) alongside multi-view reference images (left) with togglable 2D projections, rating the geometric fidelity on a 1 to 5 scale.



**Figure 10 NyeriaPlus Shape Annotations.** Examples of recordings with shape annotations. Different colors represent distinct shape instances.

7171 total qualified object bounding boxes. In the second phase, similar to 3D bounding box propagation we propagate these validated geometries to the remaining sequence recordings. Here, a 3D shape is transferred from the basemap to a target recording if and only if the 3D IoU between the source and target bounding boxes is near perfect, ensuring strict spatial consistency. Finally, because this strict IoU threshold naturally disqualifies many potential transfers, the third phase addresses the remaining unpopulated bounding boxes. We run the full ShapeR inference and manual annotation protocol on these residual objects, retaining only the meshes that pass the established quality threshold.

### 3.5 Additional modalities for release

In NyeriaPlus, we additionally release several data modalities that were not included in prior releases. First, we release 47 new basemap recordings captured with Project Aria glasses, one per indoor venue. These basemaps serve as the foundation for the 3D OBB and object-shape annotations described in [Sec. 3](#). Second, we release all wristband videos. Each wristband provides one RGB stream and two grayscale streams from forward-facing cameras. In total, this corresponds to more than 600 hours of wrist-perspective video. As with the Aria glasses footage, all wristband videos are anonymized. Third, we release the full audio recordings from

the Project Aria glasses, including both participants and observers, totaling more than 600 hours. Finally, we backfill the original release with updated online calibration results, including RGB camera calibration. We find that the improved online calibration yields more accurate downstream 3D reconstruction.

## 4 Conclusion

We introduced NymeriaPlus, an enriched version of the Nymeria dataset that substantially expands its utility for egocentric human motion understanding and scene-aware reasoning. NymeriaPlus provides improved full-body motion annotations in widely used parametric formats (MHR and SMPL), large-scale 3D/2D oriented bounding box annotations for indoor objects and structural elements under both closed- and open-set taxonomies, and instance-level 3D object reconstructions. In addition, we release previously withheld modalities—including basemap scans, wristband videos, and audio—together with updated calibration, enabling more comprehensive multimodal and geometric studies.

By combining accurate motion with dense scene context at scale, NymeriaPlus bridges a key gap between in-the-wild egocentric perception, interaction modeling, and embodied AI. We hope this release will support a broad range of future research, including environment-aware motion tracking and synthesis, open-world 3D object detection, fine-grained human–scene interaction analysis, and multimodal learning.

## References

- [1] Apple Vision Pro. <https://www.apple.com/apple-vision-pro/>. (3)
- [2] Microsoft HoloLens. <https://learn.microsoft.com/en-us/hololens/>. (3)
- [3] Pytorch library. <https://pytorch.org/>. (7)
- [4] Meta Quest. <https://www.meta.com/quest/>. (3)
- [5] Ray-Ban Meta smart glasses. <https://www.meta.com/smart-glasses/>. (3)
- [6] HTC VIVE. <vive.com>. (3)
- [7] Vuzix smart glasses. <https://www.vuzix.com/pages/smart-glasses>. (3)
- [8] Henrik Aanaes, Rasmus Ramsbøl Jensen, George Vogiatzis, Engin Tola, and Anders Bjarholm Dahl. Large-scale data for multiple-view stereopsis. *International Journal of Computer Vision*, 120(2):153–168, 2016. (4)
- [9] Advanced Computing Center for the Arts and Design. ACCAD MoCap Dataset. <https://accad.osu.edu/research/motion-lab/mocap-system-and-data>. (3)
- [10] Adel Ahmadyan, Liangkai Zhang, Artsiom Ablavatski, Jianing Wei, and Matthias Grundmann. Objectron: A large scale dataset of object-centric videos in the wild with pose annotations. In *IEEE/CVF Conference on Computer Vision and Pattern Recognition (CVPR)*, 2021. (2, 3)
- [11] Hiroyasu Akada, Jian Wang, Soshi Shimada, Masaki Takahashi, Christian Theobalt, and Vladislav Golyanik. UnrealEgo: A new dataset for robust egocentric 3d human motion capture. In *European Conference on Computer Vision (ECCV)*, 2022. (2, 3)
- [12] Ijaz Akhter and Michael J. Black. Pose-conditioned joint angle limits for 3D human pose reconstruction. In *IEEE/CVF Conference on Computer Vision and Pattern Recognition (CVPR)*, June 2015. (3)
- [13] Joao Pedro Araujo, Jiaman Li, Karthik Vetrivel, Rishi Agarwal, Deepak Gopinath, Jiajun Wu, Alexander Clegg, and C. Karen Liu. CIRCLE: Capture in rich contextual environments. *IEEE/CVF Conference on Computer Vision and Pattern Recognition (CVPR)*, 2023. (2, 3)
- [14] Andreas Aristidou, Ariel Shamir, and Yiorgos Chrysanthou. Digital dance ethnography: Organizing large dance collections. *J. Comput. Cult. Herit.*, 12(4), November 2019. ISSN 1556-4673. doi: 10.1145/3344383. <https://doi.org/10.1145/3344383>. (3)
- [15] Armen Avetisyan, Manuel Dahnert, Angela Dai, Manolis Savva, Angel X Chang, and Matthias Nießner. Scan2cad: Learning cad model alignment in rgb-d scans. In *Proceedings of the IEEE/CVF Conference on computer vision and pattern recognition*, pages 2614–2623, 2019. (4)
- [16] Armen Avetisyan, Christopher Xie, Henry Howard-Jenkins, Tsun-Yi Yang, Samir Aroudj, Suvam Patra, Fuyang Zhang, Duncan Frost, Luke Holland, Campbell Orme, et al. Scenescrypt: Reconstructing scenes with an autoregressive structured language model. In *European Conference on Computer Vision (ECCV)*, pages 247–263. Springer, 2024. (2)
- [17] Armen Avetisyan, Christopher Xie, Henry Howard-Jenkins, Tsun-Yi Yang, Samir Aroudj, Suvam Patra, Fuyang Zhang, Duncan Frost, Luke Holland, Campbell Orme, et al. Scenescrypt: Reconstructing scenes with an autoregressive structured language model. In *European Conference on Computer Vision*, pages 247–263. Springer, 2024. (4)
- [18] Yutong Bai, Danny Tran, Amir Bar, Yann LeCun, Trevor Darrell, and Jitendra Malik. Whole-body conditioned egocentric video prediction, 2025. <https://arxiv.org/abs/2506.21552>. (4)
- [19] Sven Bambach, Stefan Lee, David Crandall, and Chen Yu. Lending a hand: Detecting hands and recognizing activities in complex egocentric interactions. In *IEEE/CVF International Conference on Computer Vision (ICCV)*, pages 196–204, 2015. (2)
- [20] Prithviraj Banerjee, Sindi Shkodrani, Pierre Moulon, Shreyas Hampali, Shangchen Han, Fan Zhang, Linguang Zhang, Jade Fountain, Edward Miller, Selen Basol, Richard Newcombe, Robert Wang, Jakob Julian Engel, and Tomas Hodan. HOT3D: Hand and object tracking in 3D from egocentric multi-view videos. *IEEE/CVF Conference on Computer Vision and Pattern Recognition (CVPR)*, 2025. (2, 3)

- [21] Fabien Baradel\*, Matthieu Armando, Salma Galaoui, Romain Brégier, Philippe Weinzaepfel, Grégory Rogez, and Thomas Lucas\*. Multi-hmr: Multi-person whole-body human mesh recovery in a single shot. In *European Conference on Computer Vision (ECCV)*, 2024. (3)
- [22] German Barquero, Nadine Bertsch, Manojkumar Marramreddy, Carlos Chacón, Filippo Arcadu, Ferran Rigual, Nicky Sijia He, Cristina Palmero, Sergio Escalera, Yuting Ye, and Robin Kips. From sparse signal to smooth motion: Real-time motion generation with rolling prediction models. In *IEEE/CVF Conference on Computer Vision and Pattern Recognition (CVPR)*, pages 1850–1860, June 2025. (2)
- [23] Gilad Baruch, Zhuoyuan Chen, Ilya Kostrikov, Shuaibin Ma, Zhuo Yang, et al. Arkitscenes: A diverse real-world dataset for 3d indoor reconstruction. In *NeurIPS Datasets and Benchmarks Track*, 2021. (3)
- [24] Bharat Lal Bhatnagar, Xianghui Xie, Ilya Petrov, Cristian Sminchisescu, Christian Theobalt, and Gerard Pons-Moll. BEHAVE: Dataset and method for tracking human object interactions. In *IEEE/CVF Conference on Computer Vision and Pattern Recognition (CVPR)*. IEEE, jun 2022. (2)
- [25] Michael J. Black, Priyanka Patel, Joachim Tesch, and Jinlong Yang. BEDLAM: A synthetic dataset of bodies exhibiting detailed lifelike animated motion. In *IEEE/CVF Conference on Computer Vision and Pattern Recognition (CVPR)*, pages 8726–8737, June 2023. doi: 10.1109/CVPR52729.2023.00843. <https://bedlam.is.tue.mpg.de/>. (2, 3)
- [26] Federica Bogo, Javier Romero, Gerard Pons-Moll, and Michael J. Black. Dynamic FAUST: Registering human bodies in motion. In *IEEE Conf. on Computer Vision and Pattern Recognition (CVPR)*, July 2017. (3)
- [27] Samarth Brahmabhatt, Cusuh Ham, Charles C. Kemp, and James Hays. ContactDB: Analyzing and predicting grasp contact via thermal imaging. In *IEEE/CVF Conference on Computer Vision and Pattern Recognition (CVPR)*, 2019. <https://contactdb.cc.gatech.edu>. (3)
- [28] Björn Braun, Rayan Armani, Manuel Meier, Max Moebus, and Christian Holz. egoppg: Heart rate estimation from eye-tracking cameras in egocentric systems to benefit downstream vision tasks, 2025. <https://arxiv.org/abs/2502.20879>. (3)
- [29] Garrick Brazil, Abhinav Kumar, Julian Straub, Nikhila Dzadzhu, Justin Johnson, and Nikhila Ravi. Omni3d: A large benchmark and model for 3d object detection in the wild. In *IEEE/CVF Conference on Computer Vision and Pattern Recognition (CVPR)*, 2023. (3, 8)
- [30] Zhongang Cai, Wanqi Yin, Ailing Zeng, Chen Wei, Qingping Sun, Wang Yanjun, Hui En Pang, Haiyi Mei, Mingyuan Zhang, Lei Zhang, et al. Smpler-x: Scaling up expressive human pose and shape estimation. *Advances in Neural Information Processing Systems (NeurIPS)*, 36:11454–11468, 2023. (3)
- [31] Carnegie Mellon University. CMU MoCap Dataset. <http://mocap.cs.cmu.edu>. (3)
- [32] Angel Chang, Angela Dai, Thomas Funkhouser, Maciej Halber, Matthias Niessner, Manolis Savva, Shuran Song, Andy Zeng, and Yinda Zhang. Matterport3d: Learning from rgb-d data in indoor environments. *arXiv preprint arXiv:1709.06158*, 2017. (4)
- [33] Angel X Chang, Thomas Funkhouser, Leonidas Guibas, Pat Hanrahan, Qixing Huang, Zimo Li, Silvio Savarese, Manolis Savva, Shuran Song, Hao Su, et al. Shapenet: An information-rich 3d model repository. *arXiv preprint arXiv:1512.03012*, 2015. (4)
- [34] Yu-Wei Chao, Wei Yang, Yu Xiang, Pavlo Molchanov, Ankur Handa, Jonathan Tremblay, Yashraj S. Narang, Karl Van Wyk, Umar Iqbal, Stan Birchfield, Jan Kautz, and Dieter Fox. DexYCB: A benchmark for capturing hand grasping of objects. In *IEEE/CVF Conference on Computer Vision and Pattern Recognition (CVPR)*, 2021. (2)
- [35] Anargyros Chatzitofis, Leonidas Saroglou, Prodromos Boutis, Petros Drakoulis, Nikolaos Zioulis, Shishir Subramanyam, Bart Kevelham, Caecilia Charbonnier, Pablo Cesar, Dimitrios Zarpalas, et al. Human4d: A human-centric multimodal dataset for motions and immersive media. *IEEE Access*, 8:176241–176262, 2020. (3)
- [36] Jasmine Collins, Shubham Goel, Kenan Deng, Achleshwar Luthra, Leon Xu, Erhan Gundogdu, Xi Zhang, Tomas F Yago Vicente, Thomas Dideriksen, Himanshu Arora, Matthieu Guillaumin, and Jitendra Malik. Abo: Dataset and benchmarks for real-world 3d object understanding. *CVPR*, 2022. (4)
- [37] Angela Dai, Angel X Chang, Manolis Savva, Maciej Halber, Thomas Funkhouser, and Matthias Nießner. Scannet: Richly-annotated 3d reconstructions of indoor scenes. In *Proceedings of the IEEE conference on computer vision and pattern recognition*, pages 5828–5839, 2017. (4)

- [38] Angela Dai, Angel X. Chang, Manolis Savva, Maciej Halber, Thomas Funkhouser, and Matthias Nießner. Scannet: Richly-annotated 3d reconstructions of indoor scenes. In *IEEE/CVF Conference on Computer Vision and Pattern Recognition (CVPR)*, 2017. (2, 3)
- [39] Dima Damen, Hazel Doughty, Giovanni Maria Farinella, Sanja Fidler, Antonino Furnari, Evangelos Kazakos, Davide Moltisanti, Jonathan Munro, Toby Perrett, Will Price, and Michael Wray. Scaling egocentric vision: The epic-kitchens dataset. In *European Conference on Computer Vision (ECCV)*, 2018. (2)
- [40] Dima Damen, Hazel Doughty, Giovanni Maria Farinella, , Antonino Furnari, Jian Ma, Evangelos Kazakos, Davide Moltisanti, Jonathan Munro, Toby Perrett, Will Price, and Michael Wray. Rescaling egocentric vision. *CoRR*, abs/2006.13256, 2020. (2)
- [41] Matt Deitke, Ruoshi Liu, Matthew Wallingford, Huong Ngo, Oscar Michel, Aditya Kusupati, Alan Fan, Christian Laforte, Vikram Voleti, Samir Yitzhak Gadre, Eli VanderBilt, Aniruddha Kembhavi, Carl Vondrick, Georgia Gkioxari, Kiana Ehsani, Ludwig Schmidt, and Ali Farhadi. Objaverse-xl: a universe of 10m+ 3d objects. In *Advances in Neural Information Processing Systems (NeurIPS)*, NIPS '23, Red Hook, NY, USA, 2023. Curran Associates Inc. (2)
- [42] Matt Deitke, Ruoshi Liu, Matthew Wallingford, Huong Ngo, Oscar Michel, Aditya Kusupati, Alan Fan, Christian Laforte, Vikram Voleti, Samir Yitzhak Gadre, et al. Objaverse-xl: A universe of 10m+ 3d objects. *Advances in Neural Information Processing Systems*, 36:35799–35813, 2023. (4)
- [43] Matt Deitke, Dustin Schwenk, Jordi Salvador, Luca Weihs, Oscar Michel, Eli VanderBilt, Ludwig Schmidt, Kiana Ehsani, Aniruddha Kembhavi, and Ali Farhadi. Objaverse: A universe of annotated 3d objects. In *Proceedings of the IEEE/CVF conference on computer vision and pattern recognition*, pages 13142–13153, 2023. (4)
- [44] Matt Deitke, Dustin Schwenk, Jordi Salvador, Luca Weihs, Oscar Michel, Eli VanderBilt, Ludwig Schmidt, Kiana Ehsani, Aniruddha Kembhavi, and Ali Farhadi. Objaverse: A universe of annotated 3d objects. In *IEEE/CVF Conference on Computer Vision and Pattern Recognition (CVPR)*, pages 13142–13153, 2023. (2)
- [45] Zhao Dong, Ka Chen, Zhaoyang Lv, Hong-Xing Yu, Yunzhi Zhang, Cheng Zhang, Yufeng Zhu, Stephen Tian, Zhengqin Li, Geordie Moffatt, Sean Christofferson, James Fort, Xiaqing Pan, Mingfei Yan, Jiajun Wu, Carl Yuheng Ren, and Richard Newcombe. Digital twin catalog: A large-scale photorealistic 3d object digital twin dataset. In *IEEE/CVF Conference on Computer Vision and Pattern Recognition (CVPR)*, pages 753–763, June 2025. (2, 3)
- [46] Laura Downs, Anthony Francis, Nate Koenig, Brandon Kinman, Ryan Hickman, Krista Reymann, Thomas B McHugh, and Vincent Vanhoucke. Google scanned objects: A high-quality dataset of 3d scanned household items. In *2022 International Conference on Robotics and Automation (ICRA)*, pages 2553–2560. Ieee, 2022. (4)
- [47] Matteo Dunnhofer, Antonino Furnari, Giovanni Maria Farinella, and Christian Micheloni. Visual object tracking in first person vision. *International Journal of Computer Vision*, 2022. (2)
- [48] Jakob Engel, Kiran Somasundaram, Michael Goesele, Albert Sun, Alexander Gamino, Andrew Turner, Arjang Talattof, Arnie Yuan, Bilal Souti, Brigid Meredith, Cheng Peng, Chris Sweeney, Cole Wilson, Dan Barnes, Daniel DeTone, David Caruso, Derek Valleroy, Dinesh Gajipalli, Duncan Frost, Edward Miller, Elias Mueggler, Evgeniy Oleinik, Fan Zhang, Guruprasad Somasundaram, Gustavo Solaira, Harry Lanaras, Henry Howard-Jenkins, Huixuan Tang, Hyo Jin Kim, Jaime Rivera, Ji Luo, Jing Dong, Julian Straub, Kevin Bailey, Kevin Eickenhoff, Lingni Ma, Luis Pesqueira, Mark Schwesinger, Maurizio Monge, Nan Yang, Nick Charron, Nikhil Raina, Omkar Parkhi, Peter Borschowa, Pierre Moulon, Prince Gupta, Raul Mur-Artal, Robbie Pennington, Sachin Kulkarni, Sagar Miglani, Santosh Gondi, Saransh Solanki, Sean Diener, Shangyi Cheng, Simon Green, Steve Saarinen, Suvam Patra, Tassos Mourikis, Thomas Whelan, Tripti Singh, Vasileios Balntas, Vijay Baiyya, Wilson Dreewes, Xiaqing Pan, Yang Lou, Yipu Zhao, Yusuf Mansour, Yuyang Zou, Zhaoyang Lv, Zijian Wang, Mingfei Yan, Carl Ren, Renzo De Nardi, and Richard Newcombe. Project Aria: A new tool for egocentric multi-modal AI research, 2023. (2, 3, 4, 5)
- [49] Ke Fan, Shunlin Lu, Minyue Dai, Runyi Yu, Lixing Xiao, Zhiyang Dou, Junting Dong, Lizhuang Ma, and Jingbo Wang. Go to zero: Towards zero-shot motion generation with million-scale data. In *IEEE/CVF International Conference on Computer Vision (ICCV)*, 2025. (2, 3)
- [50] Aaron Ferguson, Ahmed A. A. Osman, Berta Bescos, Carsten Stoll, Chris Twigg, Christoph Lassner, David Otte, Eric Vignola, Fabian Prada, Federica Bogo, Igor Santesteban, Javier Romero, Jenna Zarate, Jeongseok Lee, Jinyung Park, Jinlong Yang, John Doublestein, Kishore Venkateshan, Kris Kitani, Ladislav Kavan, Marco Dal Farra, Matthew Hu, Matthew Cioffi, Michael Fabris, Michael Ranieri, Mohammad Modarres, Petr Kadlecek, Rawal Khirodkar, Rinat Abdrashitov, Romain Prévost, Roman Rajbhandari, Ronald Mallet, Russell Pearsall,

- Sandy Kao, Sanjeev Kumar, Scott Parrish, Shoou-I Yu, Shunsuke Saito, Takaaki Shiratori, Te-Li Wang, Tony Tung, Yichen Xu, Yuan Dong, Yuhua Chen, Yuanlu Xu, Yuting Ye, and Zhongshi Jiang. MHR: Momentum human rig, 2025. <https://arxiv.org/abs/2511.15586>. (1, 2, 5, 6)
- [51] Huan Fu, Bowen Cai, Lin Gao, Ling-Xiao Zhang, Jiaming Wang, Cao Li, Qixun Zeng, Chengyue Sun, Rongfei Jia, Binqiang Zhao, et al. 3d-front: 3d furnished rooms with layouts and semantics. In *Proceedings of the IEEE/CVF International Conference on Computer Vision*, pages 10933–10942, 2021. (4)
- [52] Rao Fu, Dingxi Zhang, Alex Jiang, Wanxia Fu, Austin Funk, Daniel Ritchie, and Srinath Sridhar. Gigahands: A massive annotated dataset of bimanual hand activities. In *IEEE/CVF Conference on Computer Vision and Pattern Recognition (CVPR)*, pages 17461–17474, 2025. (2)
- [53] Nima Ghorbani and Michael J. Black. SOMA: Solving optical marker-based mocap automatically. In *Proc. International Conference on Computer Vision (ICCV)*, pages 11117–11126, October 2021. (3)
- [54] Saeed Ghorbani, Kimia Mahdavian, Anne Thaler, Konrad Kording, Douglas James Cook, Gunnar Blohm, and Nikolaus F. Troje. MoVi: A large multipurpose motion and video dataset. *arXiv preprint arXiv: 2003.01888*, 2020. (3)
- [55] Kristen Grauman, Andrew Westbury, Eugene Byrne, Zachary Chavis, Antonino Furnari, Rohit Girdhar, Jackson Hamburger, Hao Jiang, Miao Liu, Xingyu Liu, Miguel Martin, Tushar Nagarajan, Ilija Radosavovic, Santhosh Kumar Ramakrishnan, Fiona Ryan, Jayant Sharma, Michael Wray, Mengmeng Xu, Eric Zhongcong Xu, Chen Zhao, Siddhant Bansal, Dhruv Batra, Vincent Cartillier, Sean Crane, Tien Do, Morrie Doulaty, Akshay Erapalli, Christoph Feichtenhofer, Adriano Fragomeni, Qichen Fu, Abrahm Gebreselasie, Cristina González, James Hillis, Xuhua Huang, Yifei Huang, Wenqi Jia, Weslie Khoo, Jáchym Kolář, Satwik Kottur, Anurag Kumar, Federico Landini, Chao Li, Yanghao Li, Zhenqiang Li, Karttikeya Mangalam, Raghava Modhugu, Jonathan Munro, Tullie Murrell, Takumi Nishiyasu, Will Price, Paola Ruiz, Merey Ramazanova, Leda Sari, Kiran Somasundaram, Audrey Southerland, Yusuke Sugano, Ruijie Tao, Minh Vo, Yuchen Wang, Xindi Wu, Takuma Yagi, Ziwei Zhao, Yunyi Zhu, Pablo Arbeláez, David Crandall, Dima Damen, Giovanni Maria Farinella, Christian Fuegen, Bernard Ghanem, Vamsi Krishna Ithapu, C. V. Jawahar, Hanbyul Joo, Kris Kitani, Haizhou Li, Richard Newcombe, Aude Oliva, Hyun Soo Park, James M. Rehg, Yoichi Sato, Jianbo Shi, Mike Zheng Shou, Antonio Torralba, Lorenzo Torresani, Mingfei Yan, and Jitendra Malik. Ego4D: Around the world in 3,000 hours of egocentric video. In *IEEE/CVF Conference on Computer Vision and Pattern Recognition (CVPR)*, pages 18995–19012, June 2022. (2)
- [56] Kristen Grauman, Andrew Westbury, Lorenzo Torresani, Kris Kitani, Jitendra Malik, Triantafyllos Afouras, Kumar Ashutosh, Vijay Baiyya, Siddhant Bansal, Bikram Boote, Eugene Byrne, Zach Chavis, Joya Chen, Feng Cheng, Fu-Jen Chu, Sean Crane, Avijit Dasgupta, Jing Dong, Maria Escobar, Cristhian Forigua, Abrahm Gebreselasie, Sanjay Haresh, Jing Huang, Md Mohaiminul Islam, Suyog Jain, Rawal Khirodkar, Devansh Kukreja, Kevin J Liang, Jia-Wei Liu, Sagnik Majumder, Yongsen Mao, Miguel Martin, Effrosyni Mavroudi, Tushar Nagarajan, Francesco Ragusa, Santhosh Kumar Ramakrishnan, Luigi Seminara, Arjun Somayazulu, Yale Song, Shan Su, Zihui Xue, Edward Zhang, Jinxu Zhang, Angela Castillo, Changan Chen, Xinzhu Fu, Ryosuke Furuta, Cristina Gonzalez, Prince Gupta, Jiabo Hu, Yifei Huang, Yiming Huang, Weslie Khoo, Anush Kumar, Robert Kuo, Sach Lakhavani, Miao Liu, Mi Luo, Zhengyi Luo, Brighid Meredith, Austin Miller, Oluwatumininu Oguntola, Xiaqing Pan, Penny Peng, Shraman Pramanick, Merey Ramazanova, Fiona Ryan, Wei Shan, Kiran Somasundaram, Chenan Song, Audrey Southerland, Masatoshi Tateno, Huiyu Wang, Yuchen Wang, Takuma Yagi, Mingfei Yan, Xitong Yang, Zecheng Yu, Shengxin Cindy Zha, Chen Zhao, Ziwei Zhao, Zhifan Zhu, Jeff Zhuo, Pablo Arbelaez, Gedas Bertasius, David Crandall, Dima Damen, Jakob Engel, Giovanni Maria Farinella, Antonino Furnari, Bernard Ghanem, Judy Hoffman, C. V. Jawahar, Richard Newcombe, Hyun Soo Park, James M. Rehg, Yoichi Sato, Manolis Savva, Jianbo Shi, Mike Zheng Shou, and Michael Wray. Ego-Exo4D: Understanding skilled human activity from first- and third-person perspectives. In *IEEE/CVF Conference on Computer Vision and Pattern Recognition (CVPR)*, 2024. (2, 3)
- [57] Chuan Guo, Shihao Zou, Xinxin Zuo, Sen Wang, Wei Ji, Xingyu Li, and Li Cheng. Generating diverse and natural 3d human motions from text. In *IEEE/CVF Conference on Computer Vision and Pattern Recognition (CVPR)*, pages 5152–5161, June 2022. (3)
- [58] Vladimir Guzov, Aymen Mir, Torsten Sattler, and Gerard Pons-Moll. Human positioning system (hps): 3d human pose estimation and self-localization in large scenes from body-mounted sensors. In *IEEE/CVF Conference on Computer Vision and Pattern Recognition (CVPR)*, pages 4318–4329, 2021. (3)
- [59] Vladimir Guzov, Yifeng Jiang, Fangzhou Hong, Gerard Pons-Moll, Richard Newcombe, C Karen Liu, Yuting Ye, and Lingni Ma. HMD<sup>2</sup>: Environment-aware motion generation from single egocentric head-mounted device. In *International Conference on 3D Vision (3DV)*, pages 1394–1405. IEEE, 2025. (4)

- [60] Rishi Hazra, Brian Chen, Akshara Rai, Nitin Kamra, and Ruta Desai. Egotv: Egocentric task verification from natural language task descriptions. In *IEEE/CVF International Conference on Computer Vision (ICCV)*, pages 15417–15429, October 2023. (2)
- [61] Fabian Helm, Nikolaus Troje, Mathias Reiser, and Jörn Munzert. Bewegungsanalyse getäuschter und nicht-getäuschter 7m-würfe im handball. 01 2015. (3)
- [62] Fangzhou Hong, Vladimir Guzov, Hyo Jin Kim, Yuting Ye, Richard Newcombe, Ziwei Liu, and Lingni Ma. EgoIm: Multi-modal language model of egocentric motions. In *IEEE/CVF Conference on Computer Vision and Pattern Recognition (CVPR)*, pages 5344–5354, June 2025. (4)
- [63] Ryan Hoque, Peide Huang, David J. Yoon, Mouli Sivapurapu, and Jian Zhang. Egodex: Learning dexterous manipulation from large-scale egocentric video, 2025. <https://arxiv.org/abs/2505.11709>. (2, 3)
- [64] Ludovic Hoyet, Kenneth Ryall, Rachel McDonnell, and Carol O’Sullivan. Sleight of hand: Perception of finger motion from reduced marker sets. In *Proceedings of the ACM SIGGRAPH Symposium on Interactive 3D Graphics and Games*, pages 79–86, 2012. doi: 10.1145/2159616.2159629. (3)
- [65] Zhening Huang, Xiaoyang Wu, Fangcheng Zhong, Hengshuang Zhao, Matthias Nießner, and Joan Lasenby. Litereality: Graphics-ready 3d scene reconstruction from rgb-d scans, 2025. <https://arxiv.org/abs/2507.02861>. (4)
- [66] Ahad Jawaid and Yu Xiang. Openego: A large-scale multimodal egocentric dataset for dexterous manipulation. *arXiv preprint arXiv:2509.05513*, 2025. (2)
- [67] Nan Jiang, Zhiyuan Zhang, Hongjie Li, Xiaoxuan Ma, Zan Wang, Yixin Chen, Tengyu Liu, Yixin Zhu, and Siyuan Huang. Scaling up dynamic human-scene interaction modeling. In *IEEE/CVF Conference on Computer Vision and Pattern Recognition (CVPR)*, pages 1737–1747, June 2024. (2, 3)
- [68] Hanbyul Joo, Hao Liu, Lei Tan, Lin Gui, Bart Nabbe, Iain Matthews, Takeo Kanade, Shohei Nobuhara, and Yaser Sheikh. Panoptic studio: A massively multiview system for social motion capture. In *IEEE/CVF International Conference on Computer Vision (ICCV)*, pages 3334–3342, 2015. (3)
- [69] Simar Kareer, Dhruv Patel, Ryan Punamiya, Pranay Mathur, Shuo Cheng, Chen Wang, Judy Hoffman, and Danfei Xu. Egomimic: Scaling imitation learning via egocentric video. In *IEEE International Conference on Robotics and Automation (ICRA)*, pages 13226–13233. IEEE, 2025. (3)
- [70] Manuel Kaufmann, Yi Zhao, Chengcheng Tang, Lingling Tao, Christopher Twigg, Jie Song, Robert Wang, and Otmar Hilliges. Em-pose: 3d human pose estimation from sparse electromagnetic trackers. In *IEEE/CVF International Conference on Computer Vision (ICCV)*, pages 11510–11520, 2021. (3)
- [71] Manuel Kaufmann, Jie Song, Chen Guo, Kaiyue Shen, Tianjian Jiang, Chengcheng Tang, Juan José Zárate, and Otmar Hilliges. Emdb: The electromagnetic database of global 3d human pose and shape in the wild. In *IEEE/CVF International Conference on Computer Vision (ICCV)*, pages 14632–14643, 2023. (3)
- [72] Rawal Khirodkar, Aayush Bansal, Lingni Ma, Richard Newcombe, Minh Vo, and Kris Kitani. EgoHumans: An egocentric 3d multi-human benchmark. In *IEEE/CVF International Conference on Computer Vision (ICCV)*, 2023. (2, 3)
- [73] Rawal Khirodkar, Jyun-Ting Song, Jinkun Cao, Zhengyi Luo, and Kris Kitani. Harmony4d: A video dataset for in-the-wild close human interactions. In A. Globerson, L. Mackey, D. Belgrave, A. Fan, U. Paquet, J. Tomczak, and C. Zhang, editors, *Advances in Neural Information Processing Systems (NeurIPS)*, volume 37, pages 107270–107285. Curran Associates, Inc., 2024. doi: 10.52202/079017-3407. [https://proceedings.neurips.cc/paper\\_files/paper/2024/file/c20b843d0c6b1b40a8e6eb9a44e719c9-Paper-Datasets\\_and\\_Benchmarks\\_Track.pdf](https://proceedings.neurips.cc/paper_files/paper/2024/file/c20b843d0c6b1b40a8e6eb9a44e719c9-Paper-Datasets_and_Benchmarks_Track.pdf). (2, 3)
- [74] Jeonghwan Kim, Jisoo Kim, Jeonghyeon Na, and Hanbyul Joo. Parahome: Parameterizing everyday home activities towards 3d generative modeling of human-object interactions, 2024. (2, 3)
- [75] Tzofi Klinghoffer, Siddharth Somasundaram, Xiaoyu Xiang, Yuchen Fan, Christian Richardt, Akshat Dave, Ramesh Raskar, and Rakesh Ranjan. Shoot-Bounce-3D: Single-shot occlusion-aware 3D from lidar by decomposing two-bounce light. In *ACM SIGGRAPH Asia Conference Proceedings*, 2025. <https://shoot-bounce-3d.github.io>. (2)
- [76] Franziska Krebs, Andre Meixner, Isabel Patzer, and Tamim Asfour. The KIT bimanual manipulation dataset. In *IEEE/RAS International Conference on Humanoid Robots (Humanoids)*, pages 499–506, 2021. (3)

- [77] Anusha Krishnan, Shaohui Liu, Paul-Edouard Sarlin, Oscar Gentilhomme, David Caruso, Maurizio Monge, Richard Newcombe, Jakob Engel, and Marc Pollefeys. Benchmarking egocentric visual-inertial slam at city scale. In *IEEE/CVF International Conference on Computer Vision (ICCV)*, 2025. (2, 3)
- [78] Taein Kwon, Bugra Tekin, Jan Stühmer, Federica Bogo, and Marc Pollefeys. H2o: Two hands manipulating objects for first person interaction recognition. In *Proceedings of the IEEE/CVF international conference on computer vision*, pages 10138–10148, 2021. (2)
- [79] Justin Lazarow, David Griffiths, Gefen Kohavi, Francisco Crespo, and Afshin Dehghan. Cubify anything: Scaling indoor 3d object detection. In *IEEE/CVF Conference on Computer Vision and Pattern Recognition (CVPR)*, pages 22225–22233, 2025. (3)
- [80] Jiye Lee and Hanbyul Joo. Mocap everyone everywhere: Lightweight motion capture with smartwatches and a head-mounted camera. In *IEEE/CVF Conference on Computer Vision and Pattern Recognition (CVPR)*, pages 1091–1100, 2024. (3)
- [81] Gen Li, Kaifeng Zhao, Siwei Zhang, Xiaozhong Lyu, Mihai Dusmanu, Yan Zhang, Marc Pollefeys, and Siyu Tang. Egogen: An egocentric synthetic data generator. In *IEEE/CVF Conference on Computer Vision and Pattern Recognition (CVPR)*, pages 14497–14509, 2024. (3)
- [82] Yin Li, Miao Liu, and James M Rehg. In the eye of beholder: Joint learning of gaze and actions in first person video. In *European Conference on Computer Vision (ECCV)*, pages 619–635, 2018. (2)
- [83] Yunzhi Li, Vimal Mollyn, Kuang Yuan, and Patrick Carrington. Wheelposer: Sparse-imu based body pose estimation for wheelchair users. In *Proceedings of the 26th International ACM SIGACCESS Conference on Computers and Accessibility*, pages 1–17, 2024. (3)
- [84] Jing Lin, Ailing Zeng, Shunlin Lu, Yuanhao Cai, Ruimao Zhang, Haoqian Wang, and Lei Zhang. Motion-X: A large-scale 3d expressive whole-body human motion dataset. *Advances in Neural Information Processing Systems (NeurIPS)*, 36:25268–25280, 2023. (2, 3)
- [85] Zhaojiang Lin, Yong Xu, Kai Sun, Jing Zheng, Yin Huang, Surya Teja Appini, Krish Narang, Renjie Tao, Ishan Kapil Jain, Siddhant Arora, Ruizhi Li, Yiteng Huang, Kaushik Patnaik, Wenfang Xu, Suwon Shon, Yue Liu, Ahmed A Aly, Anuj Kumar, Florian Metze, and Xin Luna Dong. Wearvox: An egocentric multichannel voice assistant benchmark for wearables, 2025. <https://arxiv.org/abs/2601.02391>. (2)
- [86] Xingchen Liu, Piyush Tayal, Jianyuan Wang, Jesus Zarzar, Tom Monnier, Konstantinos Tertikas, Jiali Duan, Antoine Toisoul, Jason Y Zhang, Natalia Neverova, et al. Uncommon objects in 3d. In *Proceedings of the IEEE/CVF Conference on Computer Vision and Pattern Recognition*, pages 14102–14113, 2025. (4)
- [87] Matthew Loper, Naureen Mahmood, Javier Romero, Gerard Pons-Moll, and Michael J. Black. SMPL: a skinned multi-person linear model. *ACM Transactions on Graphics*, 34(6), November 2015. ISSN 0730-0301. doi: 10.1145/2816795.2818013. <https://doi.org/10.1145/2816795.2818013>. (1, 2, 3, 5, 6)
- [88] Matthew Loper, Naureen Mahmood, Javier Romero, Gerard Pons-Moll, and Michael J. Black. *SMPL: A Skinned Multi-Person Linear Model*. Association for Computing Machinery, New York, NY, USA, 1 edition, 2023. ISBN 9798400708978. <https://doi.org/10.1145/3596711.3596800>. (2, 3)
- [89] Matthew M. Loper, Naureen Mahmood, and Michael J. Black. MoSh: Motion and shape capture from sparse markers. *ACM Transactions on Graphics, (Proc. SIGGRAPH Asia)*, 33(6):220:1–220:13, November 2014. doi: 10.1145/2661229.2661273. <http://doi.acm.org/10.1145/2661229.2661273>. (3)
- [90] Eyes JAPAN Co. Ltd. Eyes Japan MoCap Dataset. <http://mocapdata.com>. (3)
- [91] Jiaxin Lu, Chun-Hao Paul Huang, Uttaran Bhattacharya, Qixing Huang, and Yi Zhou. HUMOTO: A 4d dataset of mocap human object interactions. In *IEEE/CVF International Conference on Computer Vision (ICCV)*, pages 10886–10897, October 2025. (2, 3)
- [92] Hao Luo, Ye Wang, Wanpeng Zhang, Sipeng Zheng, Ziheng Xi, Chaoyi Xu, Haiweng Xu, Haoqi Yuan, Chi Zhang, Yiqing Wang, Yicheng Feng, and Zongqing Lu. Being-h0.5: Scaling human-centric robot learning for cross-embodiment generalization, 2026. <https://arxiv.org/abs/2601.12993>. (2, 3)
- [93] Lingni Ma, Yuting Ye, Fangzhou Hong, Vladimir Guzov, Yifeng Jiang, Rowan Postyneni, Luis Pesqueira, Alexander Gamino, Vijay Baiyya, Hyo Jin Kim, Kevin Bailey, David Soriano Fosas, C. Karen Liu, Ziwei Liu, Jakob Engel, Renzo De Nardi, and Richard Newcombe. Nymeria: A massive collection of multimodal egocentric daily motion in the wild. In *European Conference on Computer Vision (ECCV)*, 2024. <https://arxiv.org/abs/2406.09905>. (1, 2, 3, 4, 5, 6)

- [94] Naureen Mahmood, Nima Ghorbani, Nikolaus F. Troje, Gerard Pons-Moll, and Michael J. Black. AMASS: Archive of motion capture as surface shapes. In *IEEE/CVF International Conference on Computer Vision (ICCV)*, pages 5442–5451, October 2019. (2, 3)
- [95] Christian Mandery, Ömer Terlemez, Martin Do, Nikolaus Vahrenkamp, and Tamim Asfour. The KIT whole-body human motion database. In *IEEE International Conference on Robotics and Automation (ICRA)*, pages 329–336, 2015. (3)
- [96] Christian Mandery, Ömer Terlemez, Martin Do, Nikolaus Vahrenkamp, and Tamim Asfour. Unifying representations and large-scale whole-body motion databases for studying human motion. *IEEE Transactions on Robotics*, 32(4):796–809, 2016. (3)
- [97] Karttikeya Mangalam, Raiymbek Akshulakov, and Jitendra Malik. Egoschema: A diagnostic benchmark for very long-form video language understanding. *Advances in Neural Information Processing Systems (NeurIPS)*, 36: 46212–46244, 2023. (2)
- [98] Claire McLean, Makenzie Meendering, Tristan Swartz, Orri Gabbay, Alexandra Olsen, Rachel Jacobs, Nicholas Rosen, Philippe de Bree, Tony Garcia, Gadsden Merrill, Jake Sandakly, Julia Buffalini, Neham Jain, Steven Krenn, Moneish Kumar, Dejan Markovic, Evonne Ng, Fabian Prada, Andrew Saba, Siwei Zhang, Vasu Agrawal, Tim Godisart, Alexander Richard, and Michael Zollhoefer. Embody 3d: A large-scale multimodal motion and behavior dataset, 2025. <https://arxiv.org/abs/2510.16258>. (2, 3)
- [99] AI Meta. The llama 4 herd: The beginning of a new era of natively multimodal ai innovation, 2025. (12)
- [100] Momentum library. <https://github.com/facebookresearch/momentum>. (4, 6, 7)
- [101] Movella XSens. <https://www.movella.com/motion-capture/xsens-link-specifications>. (4, 5)
- [102] M. Müller, T. Röder, M. Clausen, B. Eberhardt, B. Krüger, and A. Weber. Documentation mocap database hdm05. Technical Report CG-2007-2, Universität Bonn, June 2007. (3)
- [103] Curtis G. Northcutt, Shengxin Zha, Steven Lovegrove, and Richard Newcombe. Egocom: A multi-person multimodal egocentric communications dataset. *IEEE Transactions on Pattern Analysis and Machine Intelligence*, pages 1–12, 2020. doi: 10.1109/TPAMI.2020.3025105. (2)
- [104] Xiaqing Pan, Nicholas Charron, Yongqian Yang, Scott Peters, Thomas Whelan, Chen Kong, Omkar Parkhi, Richard Newcombe, and Yuheng Carl Ren. Aria digital twin: A new benchmark dataset for egocentric 3d machine perception. In *IEEE/CVF International Conference on Computer Vision (ICCV)*, pages 20133–20143, 2023. (2, 3)
- [105] Xiaqing Pan, Nicholas Charron, Yongqian Yang, Scott Peters, Thomas Whelan, Chen Kong, Omkar Parkhi, Richard Newcombe, and Yuheng Carl Ren. Aria digital twin: A new benchmark dataset for egocentric 3d machine perception. In *Proceedings of the IEEE/CVF International Conference on Computer Vision*, pages 20133–20143, 2023. (4)
- [106] Constantin Patsch, Jaden Goter, Joseph Greer, Lingni Ma, and Raj Sodhi. Wacu: Multi-modal wristband assistant for contextual understanding. In *IEEE/CVF International Conference on Computer Vision (ICCV)*, pages 7214–7223, 2025. (4)
- [107] Georgios Pavlakos, Vasileios Choutas, Nima Ghorbani, Timo Bolkart, Ahmed A. A. Osman, Dimitrios Tzionas, and Michael J. Black. Expressive body capture: 3D hands, face, and body from a single image. In *IEEE/CVF Conference on Computer Vision and Pattern Recognition (CVPR)*, pages 10975–10985, 2019. (3, 5, 6)
- [108] Toby Perrett, Ahmad Darkhalil, Saptarshi Sinha, Omar Emara, Sam Pollard, Kranti Parida, Kaiting Liu, Prajwal Gatti, Siddhant Bansal, Kevin Flanagan, Jacob Chalk, Zhifan Zhu, Rhodri Guerrier, Fahd Abdelazim, Bin Zhu, Davide Moltisanti, Michael Wray, Hazel Doughty, and Dima Damen. Hd-epic: A highly-detailed egocentric video dataset, 2025. <https://arxiv.org/abs/2502.04144>. (2, 3)
- [109] Nicholas Pfaff, Thomas Cohn, Sergey Zakharov, Rick Cory, and Russ Tedrake. Scenemith: Agentic generation of simulation-ready indoor scenes. *arXiv preprint arXiv:2602.09153*, 2026. (4)
- [110] Yuchen Rao, Stefan Ainetter, Sinisa Stekovic, Vincent Lepetit, and Friedrich Fraundorfer. Leveraging automatic cad annotations for supervised learning in 3d scene understanding. *arXiv preprint arXiv:2504.13580*, 2025. (4)
- [111] Nikhila Ravi, Valentin Gabeur, Yuan-Ting Hu, Ronghang Hu, Chaitanya Ryali, Tengyu Ma, Haitham Khedr, Roman Rädle, Chloe Rolland, Laura Gustafson, et al. Sam 2: Segment anything in images and videos. *arXiv preprint arXiv:2408.00714*, 2024. (12)

- [112] Jeremy Reizenstein, Roman Shapovalov, Philipp Henzler, Luca Sbordone, Patrick Labatut, and David Novotny. Common objects in 3d: Large-scale learning and evaluation of real-life 3d category reconstruction. *IEEE/CVF International Conference on Computer Vision (ICCV)*, 2021. (3)
- [113] Mike Roberts, Jason Ramapuram, Anurag Ranjan, Atulit Kumar, Miguel Angel Bautista, Nathan Paczan, Russ Webb, and Joshua M Susskind. Hypersim: A photorealistic synthetic dataset for holistic indoor scene understanding. In *Proceedings of the IEEE/CVF international conference on computer vision*, pages 10912–10922, 2021. (4)
- [114] Yu Rong, Takaaki Shiratori, and Hanbyul Joo. Frankmocap: A monocular 3d whole-body pose estimation system via regression and integration. In *IEEE/CVF International Conference on Computer Vision (ICCV)*, pages 1749–1759, 2021. (3)
- [115] Paul-Edouard Sarlin, Mihai Dusmanu, Johannes L. Schönberger, Pablo Speciale, Lukas Gruber, Viktor Larsson, Ondrej Miksik, and Marc Pollefeys. LaMAR: Benchmarking Localization and Mapping for Augmented Reality. In *European Conference on Computer Vision (ECCV)*, 2022. (2)
- [116] Fadime Sener, Dibyadip Chatterjee, Daniel Sheleпов, Kun He, Dipika Singhania, Robert Wang, and Angela Yao. Assembly101: A large-scale multi-view video dataset for understanding procedural activities. In *IEEE/CVF Conference on Computer Vision and Pattern Recognition (CVPR)*, pages 21096–21106, 2022. (2)
- [117] Soshi Shimada, Vladislav Golyanik, Weipeng Xu, and Christian Theobalt. Physcap: Physically plausible monocular 3d motion capture in real time. *ACM Transactions on Graphics*, 39(6):1–16, 2020. (3)
- [118] Yawar Siddiqui, Duncan Frost, Samir Aroudj, Armen Avetisyan, Henry Howard-Jenkins, Daniel DeTone, Pierre Moulon, Qirui Wu, Zhengqin Li, Julian Straub, Richard Newcombe, and Jakob Engel. Shaper: Robust conditional 3d shape generation from casual captures, 2026. <https://arxiv.org/abs/2601.11514>. (4, 11, 12)
- [119] L. Sigal, A. Balan, and M. J. Black. HumanEva: Synchronized video and motion capture dataset and baseline algorithm for evaluation of articulated human motion. *International Journal of Computer Vision*, 87(1):4–27, March 2010. (3)
- [120] Shuran Song, Samuel P Lichtenberg, and Jianxiong Xiao. Sun rgb-d: A rgb-d scene understanding benchmark suite. In *IEEE/CVF Conference on Computer Vision and Pattern Recognition (CVPR)*, 2015. (3)
- [121] Olga Sorkine-Hornung and Michael Rabinovich. Least-squares rigid motion using svd. *Computing*, 1(1):1–5, 2017. (5, 6)
- [122] Julian Straub, Thomas Whelan, Lingni Ma, Yufan Chen, Erik Wijmans, Simon Green, Jakob J. Engel, Raul Mur-Artal, Carl Ren, Shobhit Verma, Anton Clarkson, Mingfei Yan, Brian Budge, Yajie Yan, Xiaqing Pan, June Yon, Yuyang Zou, Kimberly Leon, Nigel Carter, Jesus Briales, Tyler Gillingham, Elias Mueggler, Luis Pesqueira, Manolis Savva, Dhruv Batra, Hauke M. Strasdat, Renzo De Nardi, Michael Goesele, Steven Lovegrove, and Richard Newcombe. The Replica dataset: A digital replica of indoor spaces. *arXiv preprint arXiv:1906.05797*, 2019. (2)
- [123] Julian Straub, Thomas Whelan, Lingni Ma, Yufan Chen, Erik Wijmans, Simon Green, Jakob J Engel, Raul Mur-Artal, Carl Ren, Shobhit Verma, et al. The replica dataset: A digital replica of indoor spaces. *arXiv preprint arXiv:1906.05797*, 2019. (4)
- [124] Julian Straub, Daniel DeTone, Tianwei Shen, Nan Yang, Chris Sweeney, and Richard Newcombe. Efm3d: A benchmark for measuring progress towards 3d egocentric foundation models. *arXiv preprint arXiv:2406.10224*, 2024. (3, 8, 10, 25)
- [125] Chi Su, Xiaoxuan Ma, Jiajun Su, and Yizhou Wang. Sat-hmr: Real-time multi-person 3d mesh estimation via scale-adaptive tokens. In *IEEE/CVF Conference on Computer Vision and Pattern Recognition (CVPR)*, pages 16796–16806, June 2025. (3)
- [126] Omid Taheri, Nima Ghorbani, Michael J. Black, and Dimitrios Tzionas. GRAB: A dataset of whole-body human grasping of objects. In *European Conference on Computer Vision (ECCV)*, 2020. <https://grab.is.tue.mpg.de>. (2, 3)
- [127] Shashank Tripathi, Lea Müller, Chun-Hao P. Huang, Taheri Omid, Michael J. Black, and Dimitrios Tzionas. 3D human pose estimation via intuitive physics. In *IEEE/CVF Conference on Computer Vision and Pattern Recognition (CVPR)*, June 2023. (3)
- [128] Nikolaus F. Troje. Decomposing biological motion: A framework for analysis and synthesis of human gait patterns. *Journal of Vision*, 2(5):2–2, September 2002. doi: 10.1167/2.5.2. (3)

- [129] Matt Trumble, Andrew Gilbert, Charles Malleson, Adrian Hilton, and John Collomosse. Total Capture: 3d human pose estimation fusing video and inertial sensors. In *2017 British Machine Vision Conference (BMVC)*, 2017. (3)
- [130] Simon Fraser University and National University of Singapore. SFU Motion Capture Database. <http://mocap.cs.sfu.ca/>. (3)
- [131] Timo Von Marcard, Roberto Henschel, Michael J Black, Bodo Rosenhahn, and Gerard Pons-Moll. Recovering accurate 3d human pose in the wild using imus and a moving camera. In *European Conference on Computer Vision (ECCV)*, pages 601–617, 2018. (3)
- [132] Jian Wang, Rishabh Dabral, Diogo Luvizon, Zhe Cao, Lingjie Liu, Thabo Beeler, and Christian Theobalt. Ego4o: Egocentric human motion capture and understanding from multi-modal input. In *IEEE/CVF Conference on Computer Vision and Pattern Recognition (CVPR)*, pages 22668–22679, 2025. (4)
- [133] Xiaofeng Wang, Kang Zhao, Feng Liu, Jiayu Wang, Guosheng Zhao, Xiaoyi Bao, Zheng Zhu, Yingya Zhang, and Xingang Wang. EgoVid-5M: A large-scale video-action dataset for egocentric video generation, 2024. <https://arxiv.org/abs/2411.08380>. (2)
- [134] Xin Wang, Taein Kwon, Mahdi Rad, Bowen Pan, Ishani Chakraborty, Sean Andrist, Dan Bohus, Ashley Feniello, Bugra Tekin, Felipe Vieira Frujeri, Neel Joshi, and Marc Pollefeys. Holoassist: an egocentric human interaction dataset for interactive ai assistants in the real world. In *IEEE/CVF International Conference on Computer Vision (ICCV)*, pages 20270–20281, October 2023. (2, 3)
- [135] Yufu Wang, Yu Sun, Priyanka Patel, Kostas Daniilidis, Michael J Black, and Muhammed Kocabas. Promptmr: Promptable human mesh recovery. *IEEE/CVF Conference on Computer Vision and Pattern Recognition (CVPR)*, 2025. (3)
- [136] Jingqiao Xiu, Fangzhou Hong, Yicong Li, Mengze Li, Wentao Wang, Sirui Han, Liang Pan, and Ziwei Liu. Egotwin: Dreaming body and view in first person, 2025. <https://arxiv.org/abs/2508.13013>. (4)
- [137] Zhen Xu, Zhengqin Li, Zhao Dong, Xiaowei Zhou, Richard Newcombe, and Zhaoyang Lv. 4dgt: Learning a 4d gaussian transformer using real-world monocular videos. 2025. (4)
- [138] Charig Yang, Samiul Alam, Shakhrul Iman Siam, Michael J Proulx, Lambert Mathias, Kiran Somasundaram, Luis Pesqueira, James Fort, Sheroze Sherifdeen, Omkar Parkhi, et al. Reading recognition in the wild. In *Advances in Neural Information Processing Systems (NeurIPS)*, 2025. (2, 3)
- [139] Dongseok Yang, Jiho Kang, Lingni Ma, Joseph Greer, Vickie Ye, and Sung-Hee Lee. Divatrack: Diverse bodies and motions from acceleration-enhanced 3-point trackers. *Computer Graphics Forum*, 43(2):e15057, 2024. doi: <https://doi.org/> (2, 3)
- [140] Jingkang Yang, Shuai Liu, Hongming Guo, Yuhao Dong, Xiamengwei Zhang, Sicheng Zhang, Pengyun Wang, Zitang Zhou, Binzhu Xie, Ziyue Wang, Bei Ouyang, Zhengyu Lin, Marco Cominelli, Zhongang Cai, Yuanhan Zhang, Peiyuan Zhang, Fangzhou Hong, Joerg Widmer, Francesco Gringoli, Lei Yang, Bo Li, and Ziwei Liu. Egolife: Towards egocentric life assistant, 2025. <https://arxiv.org/abs/2503.03803>. (2, 3)
- [141] Vickie Ye, Georgios Pavlakos, Jitendra Malik, and Angjoo Kanazawa. Decoupling human and camera motion from videos in the wild. In *IEEE/CVF Conference on Computer Vision and Pattern Recognition (CVPR)*, pages 21222–21232, 2023. (3)
- [142] Chandan Yeshwanth, Yueh-Cheng Liu, Matthias Nießner, and Angela Dai. Scannet++: A high-fidelity dataset of 3d indoor scenes. In *IEEE/CVF International Conference on Computer Vision (ICCV)*, pages 12–22, 2023. (2, 3)
- [143] Chandan Yeshwanth, Yueh-Cheng Liu, Matthias Nießner, and Angela Dai. Scannet++: A high-fidelity dataset of 3d indoor scenes. In *Proceedings of the IEEE/CVF International Conference on Computer Vision*, pages 12–22, 2023. (4)
- [144] Huangyue Yu, Baoxiong Jia, Yixin Chen, Yandan Yang, Puhao Li, Rongpeng Su, Jiaxin Li, Qing Li, Wei Liang, Song-Chun Zhu, et al. Metascenes: Towards automated replica creation for real-world 3d scans. In *Proceedings of the Computer Vision and Pattern Recognition Conference*, pages 1667–1679, 2025. (4)
- [145] Siwei Zhang, Qianli Ma, Yan Zhang, Zhiyin Qian, Taein Kwon, Marc Pollefeys, Federica Bogo, and Siyu Tang. EgoBody: Human body shape and motion of interacting people from head-mounted devices. In *European Conference on Computer Vision (ECCV)*, Oct 2022. (2, 3)

- [146] Siwei Zhang, Bharat Lal Bhatnagar, Yuanlu Xu, Alexander Winkler, Petr Kadlecek, Siyu Tang, and Federica Bogo. RoHM: Robust Human Motion Reconstruction via Diffusion. In *IEEE/CVF Conference on Computer Vision and Pattern Recognition (CVPR)*, 2024. (7)
- [147] Yuhong Zhang, Jing Lin, Ailing Zeng, Guanlin Wu, Shunlin Lu, Yurong Fu, Yuanhao Cai, Ruimao Zhang, Haoqian Wang, and Lei Zhang. Motion-X++: A large-scale multimodal 3d whole-body human motion dataset. *arXiv preprint arXiv:2501.05098*, 2025. (2, 3)
- [148] Yiming Zhao, Taein Kwon, Paul Strelci, Marc Pollefeys, and Christian Holz. Egopressure: A dataset for hand pressure and pose estimation in egocentric vision. In *IEEE/CVF Conference on Computer Vision and Pattern Recognition (CVPR)*, pages 27727–27738, June 2025. (3)
- [149] Chenchen Zhu, Fanyi Xiao, Andrés Alvarado, Yasmine Babaei, Jiabo Hu, Hichem El-Mohri, Sean Chang, Roshan Sumbaly, and Zhicheng Yan. Egoobjects: A large-scale egocentric dataset for fine-grained object understanding. In *IEEE/CVF International Conference on Computer Vision (ICCV)*, 2023. (2)
- [150] Katerina Zmolikova, Simone Merello, Kaustubh Kalgaonkar, Ju Lin, Niko Moritz, Pingchuan Ma, Ming Sun, Honglie Chen, Antoine Saliou, Stavros Petridis, et al. The chime-8 mmcs challenge: Multi-modal conversations in smart glasses. In *8th International Workshop on Speech Processing in Everyday Environments (CHiME)*, pages 7–12, 2024. (3)

# Appendix

## A Fixed-Set Taxonomy for 3D OBB Annotations

In this section, we describe the fixed-set taxonomy used to annotate commonly occurring objects (similar to the classes used in EFM3D [124]).

**Bed.** A bed is a surface intended for sleeping. This includes queen beds, bunk beds, bed frames without a mattress, mattresses without a bed frame, and cribs. A bunk bed is treated as a single object.

**Chair.** An object designed for a single person to sit on. Examples include beanbags, ottomans, three-legged chairs, and office chairs with caster wheels. Toilets are excluded because they serve a different function.

**Couch.** An object designed for one or more people to sit on, typically upholstered. Examples include L-shaped sectionals, hammocks, loveseats, and recliners. For sectional couches, annotators split the object into multiple sections to obtain tighter boxes.

**Door.** A static opening that a person can pass through and that can be closed by a door slab. Examples include closet doors, hallway entrances, shed entrances, storage-room doors, and bathroom entries. Very large doors designed for vehicles (e.g., garage doors) are excluded. This class does not include the door slab itself, which can articulate.

**Floor.** For simplicity and compatibility, we represent floors using 3D oriented bounding boxes, although planar polygons would be a more expressive representation. Annotators align the top face of each floor OBB with the underlying floor plane. For level, single-story venues, a single floor box typically covers the indoor space. For multi-floor venues, we split the floor into multiple boxes; for outdoor areas with uneven ground, we approximate the surface using piecewise-planar boxes. Annotators prioritize coverage of the ground beneath the Aria wearer so that downstream applications requiring height above ground can be supported throughout NymeriaPlus.

**Lamp/Light.** A generic class that includes both standalone lights and light fixtures. For fixtures containing a light bulb, annotators provide the largest reasonable box; for example, a ceiling fan with lights is annotated as a single object covering the entire fan. Other examples include recessed lights, chandeliers, floor lamps, and soffit lights.

**Mirror.** An object with a reflective mirror surface, including full-body mirrors, vanity mirrors, personal face mirrors, and handheld mirrors. When a stand is present, annotators annotate only the mirror surface. Groups of nearby small mirrors may be annotated with a single box.

**Table.** An object whose primary purpose is to place items on (as opposed to storing items; see **Storage/Shelf**). Examples include dining tables, coffee tables, and desks. If an ottoman is used as a coffee table rather than a footrest, we annotate it as a table.

**Wall Art / Picture Frame.** A broad class covering decorative wall-mounted items and framed media, including wall art, posters, calendars, wall flags, and photo frames (whether wall-mounted or resting on furniture). Items such as light switches, wall shelves, vents, and temporarily hung personal objects are excluded. If multiple nearby pieces clearly form a single composite artwork, they may be annotated as one object.

**Window Opening.** Similar to **Door**, this class represents the static space occupied by a closed window, rather than the window itself, which may articulate. Examples include skylights and double-pane windows. Curtains are excluded when they occlude the window. The perimeter is defined as the space just inside the outermost window casing (when present). Windows embedded in doors are excluded because they are moveable.

**Plant.** This class includes potted plants (real or artificial), flowers in vases, shrubs, and trees. For indoor plants, we include the pot or vase. Outdoors, tightly clustered vegetation is difficult to separate, so we focus on more isolated instances. For trees, we annotate the full tree when observable; otherwise, we annotate only the trunk. Vines are excluded because they are poorly approximated by a 3D OBB.

**Storage/Shelf.** An object whose primary purpose is storage. Examples include closet rods, floating shelves, wall pegboards, window ledges, cabinets (e.g., under-sink or kitchen), shoe racks, dressers, mantles, shower

nooks, built-in shelving, and toilet paper holders. For floating shelves, each shelf is annotated independently; for multi-shelf units, the entire unit is annotated as a single box. Temporary or frequently moved containers (e.g., laundry baskets, cardboard boxes, plastic tubs) are excluded.

**Screen/Display.** A digital display other than a handheld mobile phone. Examples include computer monitors, televisions, tablets, printer displays, arcade screens, and conference-room displays (including when powered off).

**Wall.** Similar to **Floor**, we approximate walls using 3D oriented bounding boxes for simplicity, although planar polygons would also be suitable. We initialize each wall as a 12 cm thick volume; annotators may adjust thickness when warranted. This class includes deck railings, pony walls, exterior siding, yard walls, fences, and angled staircase railings. Curved walls are approximated using multiple smaller segments. For walls with vaulted ceilings, we annotate a box that extends to the highest part of the wall. Columns and pillars are excluded unless they are wider than 4 feet. If an archway or cutout is part of the wall, we keep a single larger wall box that spans the opening rather than annotating sub-walls.

**Sink.** A fixed vessel for washing hands or objects, typically with a faucet (which is excluded from the annotation). Examples include bathroom vanity sinks, farmhouse kitchen sinks, and utility sinks. Exposed plumbing beneath the sink is excluded.

**Toilet.** We include the bowl and tank, but exclude the lid when it is open and extends above the tank.

**Refrigerator.** An appliance used to keep items cool, including mini fridges, wine fridges, and standalone freezers (e.g., in a garage).

**WasherDryer.** Standalone clothes washers, clothes dryers, and stackable washer–dryer towers. Dishwashers are excluded. If a door is open and extends beyond the main body, we exclude the door.

**Stairs.** We annotate each staircase as a sequence of steps. Single steps connecting subregions of a space are included (e.g., a step down to a garage). Non-walkable ledges (e.g., fireplace ledges) are excluded. For curved or angled staircases, we approximate the structure using a small number of segments.

## B Acknowledgement

We thank Nan Yang, Jiayi Jiang, Petr Kadlecek, and Jinlong Yang for dogfooding and support with human motion optimization. We also thank Dan Barnes and Raul Mur-Artal for early support on 3D bounding box annotations. We are grateful to Austin Kukay, Rowan Postyeni, Ruosha Pang, Mu Cheng, William Sun, Chen Zhang, Qinyue He, Aaron Deguzman, Yao Zhi, Luis Pesqueira, Abha Arora, and Rana Hayek for annotation support. Finally, we thank Fan Zhang, and Hauke Strasdat for general project support.